Eur. Phys. J. C 52, 93–112 (2007)
DOI 10.1140/epjc/s10052-007-0365-9

THE EUROPEAN PHYSICAL JOURNAL C

Regular Article – Theoretical Physics

Diffractive production of two ρ^0_{L} mesons in e^+e^- collisions

M. Segond[1], L. Szymanowski[1,2,3,4], S. Wallon[1,a]

[1] LPT, Université Paris-Sud – CNRS, 91405 Orsay, France
[2] Soltan Institute for Nuclear Studies, Warsaw, Poland
[3] Université de Liège, 4000 Liège, Belgium
[4] CPHT, École Polytechnique – CNRS, 91128 Palaiseau, France

Received: 15 March 2007 / Revised version: 30 April 2007 /

Abstract. We present an estimate of the cross-section for the exclusive production of a ρ^0_{L}-meson pair in e^+e^- scattering, which will be studied in the future high-energy International Linear Collider. For this aim, we complete calculations of the Born order approximation of the amplitudes $\gamma^*_{\mathrm{L,T}}(Q_1^2)\gamma^*_{\mathrm{L,T}}(Q_2^2) \to \rho^0_{\mathrm{L}}\rho^0_{\mathrm{L}}$, for arbitrary polarization of virtual photons and longitudinally polarized mesons, in the kinematical region $s \gg -t, Q_1^2, Q_2^2$. These processes are completely calculable in the hard region $Q_1^2, Q_2^2 \gg \Lambda^2_{\mathrm{QCD}}$, and we perform most of the calculations in an analytical way. The resulting cross-section turns out to be large enough for this process to be measurable with foreseen luminosity and energy, for Q_1^2 and Q_2^2 in the range of a few GeV^2.

1 Introduction

The next generation of e^+e^- colliders will offer a possibility of clean testing of QCD dynamics. By selecting events in which two vector mesons are produced with large rapidity gap, through scattering of two highly virtual photons, one is getting access to the kinematical regime in which the perturbative approach is justified. If additionally one selects the events with comparable photon virtualities, the perturbative Regge dynamics of QCD of the BFKL [1–4] type should dominate with respect to the conventional partonic evolution of DGLAP [5–9] type. Several studies of BFKL dynamics have been performed at the level of the total cross-section [10–17].

In [18] the diffractive production of two J/Ψ mesons was studied as a promising probe of the BFKL effects. Recently, we have advocated [19–24] the idea that the electroproduction of two ρ mesons in $\gamma^*\gamma^*$ offers the same advantages. In this case the virtualities of the scattered photons play the role of the hard scales. A first step in this direction was made by considering this process with longitudinally polarized photons and ρ mesons,

$$\gamma^*_{\mathrm{L}}(q_1)\gamma^*_{\mathrm{L}}(q_2) \to \rho^0_{\mathrm{L}}(k_1)\rho^0_{\mathrm{L}}(k_2)\,, \tag{1}$$

for arbitrary values of $t = (q_1 - k_1)^2$, with $s \gg -t$. The choice of longitudinal polarizations of both the scattered photons and produced vector mesons was dictated by the fact that this configuration of the lowest twist, twist 2, gives the dominant contribution in the powers of the hard scale Q^2, when $Q_1^2 \sim Q_2^2 \sim Q^2$.

The aim of this study is to complete the Born order evaluation of the cross-section of the process

$$e^+e^- \to e^+e^-\rho^0_{\mathrm{L}}\rho^0_{\mathrm{L}}\,, \tag{2}$$

illustrated in Fig. 1. We calculated contributions with remaining combinations of polarizations of virtual photons necessary to obtain all helicity amplitudes of the processes

$$\gamma^*_{\mathrm{L,T}}(q_1)\gamma^*_{\mathrm{L,T}}(q_2) \to \rho^0_{\mathrm{L}}(k_1)\rho^0_{\mathrm{L}}(k_2)\,. \tag{3}$$

Let us note that the double tagging of final leptons gives in particular the possibility to separate the contributions of various photon polarizations, entering in (2), and thus to study the corresponding parts of the cross-sections, which are computed in this paper. We are focusing here on the high-energy limit in which t-channel gluonic exchanges

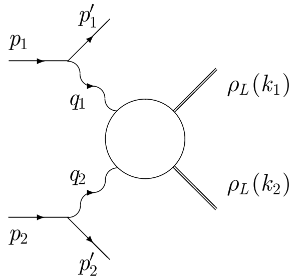

Fig. 1. Amplitude for the process $e^+e^- \to e^+e^-\rho^0_{\mathrm{L}}\rho^0_{\mathrm{L}}$

---

[a] e-mail: Samuel.Wallon@th.u-psud.fr

dominate. On the other hand, in the description of the process (2), there is a possibility that also contributions with rather small $s_{\gamma^*\gamma^*}$ have to be taken into account. In this case one should include in principle both quark and gluon exchanges. The contribution of quark exchange was analyzed in [25]. This quark-box contribution is investigated in Sect. 4.3.

We will also not consider here the case of transversally polarized ρ mesons. It would require one to deal with possible breaking of QCD factorization [26–30], although a method to overcome this problem has been proposed [31–33].

The BFKL enhancement was studied for $t = 0$ in [23, 24, 34, 35]. In this latter case, the peculiar value $t = 0$ automatically selects the longitudinally polarized photon. A dedicated study for arbitrary value of t should thus be performed to get an evaluation of BFKL enhancement effects of the Born order evaluation performed in the present paper for transversally polarized photon. This problem will not be addressed here.

2 Kinematics

The measurable cross-section for the process (2) of Fig. 1 is related to the amplitude of the process (3), illustrated in Fig. 2, through the usual flux factors for respectively transversally and longitudinally polarized photons,

$$t(y_i) = \frac{1+(1-y_i)^2}{2}\,, \quad l(y_i) = 1 - y_i\,, \tag{4}$$

where y_i $(i = 1, 2)$ are the longitudinal momentum fractions of the bremsstrahlung photons with respect to the incoming leptons. This relation reads [36]

$$\begin{aligned}
&\frac{\mathrm{d}\sigma\big(e^+e^- \to e^+e^-\rho^0_{\mathrm{L}}\rho^0_{\mathrm{L}}\big)}{\mathrm{d}y_1\,\mathrm{d}y_2\,\mathrm{d}Q_1^2\,\mathrm{d}Q_2^2}\\
&\quad = \frac{1}{y_1 y_2 Q_1^2 Q_2^2}\left(\frac{\alpha}{\pi}\right)^2 \big[l(y_1)l(y_2)\sigma\big(\gamma^*_{\mathrm{L}}\gamma^*_{\mathrm{L}} \to \rho^0_{\mathrm{L}}\rho^0_{\mathrm{L}}\big)\\
&\qquad + t(y_1)l(y_2)\sigma\big(\gamma^*_{\mathrm{T}}\gamma^*_{\mathrm{L}} \to \rho^0_{\mathrm{L}}\rho^0_{\mathrm{L}}\big)\\
&\qquad + l(y_1)t(y_2)\sigma\big(\gamma^*_{\mathrm{L}}\gamma^*_{\mathrm{T}} \to \rho^0_{\mathrm{L}}\rho^0_{\mathrm{L}}\big)\\
&\qquad + t(y_1)t(y_2)\sigma\big(\gamma^*_{\mathrm{T}}\gamma^*_{\mathrm{T}} \to \rho^0_{\mathrm{L}}\rho^0_{\mathrm{L}}\big)\big]\,.
\end{aligned} \tag{5}$$

The presence of hard scales Q_i^2 permits us to apply the collinear approximation at each $q\bar{q}\rho$-meson vertex, and the use of the distribution amplitude (DA) for describing the $q\bar{q}$ content of the ρ mesons, as illustrated in Fig. 2. In this paper, except for Sect. 4.3, the amplitude M_H will be described using the impact representation, valid at high energy, as illustrated in Fig. 3.

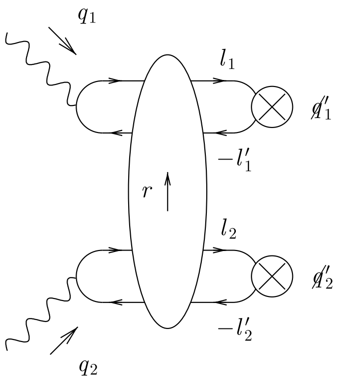

Fig. 3. The amplitude M_H in the impact representation. The *vertical blob* symbolizes the interaction of two $q\bar{q}$ dipoles through gluon exchanges at high s

Let us introduce the two light-like Sudakov vectors q'_1 and q'_2, which form a natural basis for two scattered virtual photons, which satisfy $2q'_1 \cdot q'_2 \equiv s \sim 2q_1 \cdot q_2$. The usual $s_{\gamma^*\gamma^*}$ is related to the useful auxiliary variable s by $s_{\gamma^*\gamma^*} = s - Q_1^2 - Q_2^2$. The momentum transfer in the t-channel is $r = k_1 - q_1$. In this basis, the incoming photon momenta read

$$q_1 = q'_1 - \frac{Q_1^2}{s}q'_2 \quad \text{and} \quad q_2 = q'_2 - \frac{Q_2^2}{s}q'_1\,. \tag{6}$$

The polarization vectors of longitudinally polarized photons are

$$\epsilon^{\mathrm{L}(1)}_\mu = \frac{q_{1\mu}}{Q_1} + \frac{2Q_1}{s}q'_{2\mu} \quad \text{and} \quad \epsilon^{\mathrm{L}(2)}_\mu = \frac{q_{2\mu}}{Q_2} + \frac{2Q_2}{s}q'_{1\mu}\,, \tag{7}$$

with $\epsilon^2_{\mathrm{L}(i)} = 1$ and $q_i \cdot \epsilon_{\mathrm{L}(i)} = 0$, whereas the polarization vectors of transversally polarized photons are two dimensional transverse vectors satisfying $\epsilon^2_{\mathrm{T}(i)} = -1$ $(i = 1, 2)$ and $q_i \cdot \epsilon_{\mathrm{T}(i)} = 0$.

We label the momentum of the quarks and antiquarks entering the meson wave functions as l_1 and l'_1 for the upper part of the diagram and l_2 and l'_2 for the lower part (see Fig. 3).

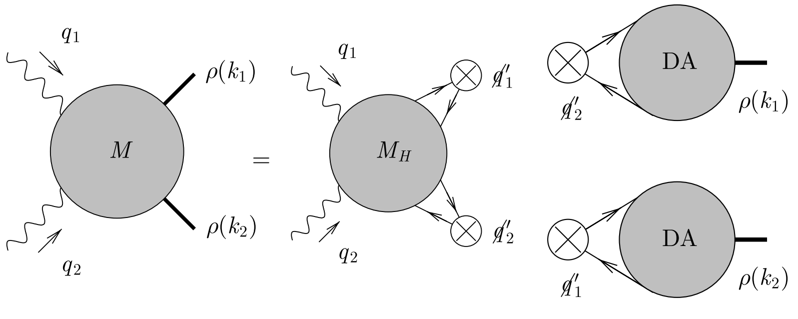

Fig. 2. The amplitude of the process $\gamma^*(Q_1)\gamma^*(Q_2) \to \rho^0_{\mathrm{L}}(k_1)\rho^0_{\mathrm{L}}(k_2)$ with the collinear factorization in the $q\bar{q}\rho$ vertices

In the basis (6), the vector meson momenta can be expanded in the form

$$k_1 = \alpha(k_1)q'_1 + \frac{\underline{r}^2}{\alpha(k_1)s}q'_2 + r_\perp\,,$$
$$k_2 = \beta(k_2)q'_2 + \frac{\underline{r}^2}{\beta(k_2)s}q'_1 - r_\perp\,. \tag{8}$$

Note that our convention is such that for any transverse vector $v_\perp$ in Minkowski space, $\underline{v}$ denotes its Euclidean form. In the following, we will treat the ρ meson as being massless. α and β are very close to unity (explicit expressions can be found in [22]), and read

$$\alpha(k_1) \simeq 1 - \frac{Q_2^2 + \underline{r}^2}{s} + O\left(\frac{1}{s^2}\right),$$
$$\beta(k_2) \simeq 1 - \frac{Q_1^2 + \underline{r}^2}{s} + O\left(\frac{1}{s^2}\right), \tag{9}$$

where $\underline{r}^2 = -r_\perp^2$. They will be replaced by 1 in the phenomenological applications of Sects. 4 and 5. In this decomposition, it is straightforward to relate $t = r^2$ to $\underline{r}^2$ through the approximate relation

$$t \sim -\frac{Q_1^2 Q_2^2}{s} - \underline{r}^2\left(1 + \frac{Q_1^2}{s} + \frac{Q_2^2}{s} + \frac{\underline{r}^2}{s}\right) \tag{10}$$

(see [22] for an exact relation). From (10) the threshold for $|t|$ is given by $|t|_{\rm min} = Q_1^2 Q_2^2/s$, corresponding to $r_\perp = 0$. In the kinematical range we are interested in, the relation (10) can be approximated as $\underline{r}^2 = -t$, as usually in the Regge limit.

The links with the e^+e^- process can be made by using the same Sudakov basis for the two incoming leptons:

$$p_1 = \frac{1}{y_1}q'_1 + y_1\frac{\underline{p}_1^2}{s}q'_2 + p_{\perp 1}$$
$$\text{and} \quad p_2 = \frac{1}{y_2}q'_2 + y_2\frac{\underline{p}_2^2}{s}q'_1 + p_{\perp 2}\,,$$
$$\underline{p}_i^2 = \frac{1-y_i}{y_i^2}Q_i^2\,. \tag{11}$$

Thus, one gets

$$s_{e^+e^-} = \frac{s}{y_1 y_2}\left(1 + \frac{(1-y_1)(1-y_2)Q_1^2 Q_2^2}{s^2}\right) - 2\underline{p}_1\cdot\underline{p}_2\,.$$

In the rest of the paper, since we keep only the dominant s contribution, we use the approximate relation $s_{e^+e^-} \sim s/(y_1 y_2)$.

3 Impact representation

The impact factor representation of the scattering amplitude for the process (3) has the form (see Fig. 4)

$$\mathcal{M} = \mathrm{i}s\int\frac{\mathrm{d}^2\underline{k}}{(2\pi)^4\underline{k}^2(\underline{r}-\underline{k})^2}\mathcal{J}^{\gamma^*_{\rm L,T}(q_1)\to\rho^0_{\rm L}(k_1)}(\underline{k},\underline{r}-\underline{k})$$
$$\times\,\mathcal{J}^{\gamma^*_{\rm L,T}(q_2)\to\rho^0_{\rm L}(k_2)}(-\underline{k},-\underline{r}+\underline{k})\,, \tag{12}$$

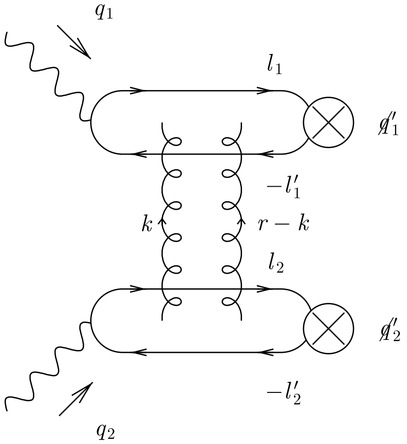

Fig. 4. Amplitude M_H at Born order. The t-channel gluons are attached to the quark lines in all possible ways

where $\mathcal{J}^{\gamma^*_{\rm L,T}(q_1)\to\rho^0_{\rm L}(k_1)}(\underline{k},\underline{r}-\underline{k})$ ($\mathcal{J}^{\gamma^*_{\rm L,T}(q_2)\to\rho^0_{\rm L}(k_2)}(\underline{k},\underline{r}-\underline{k})$) are the impact factors corresponding to the transition of $\gamma^*_{\rm L,T}(q_1)\to\rho^0_{\rm L}(k_1)$ ($\gamma^*_{\rm L,T}(q_2)\to\rho^0_{\rm L}(k_2)$) via the t-channel exchange of two gluons. The amplitude (12) calculated in Born order depends linearly on s (or $s_{\gamma^*\gamma^*}$ when neglecting terms of order Q_i^2/s) as the impact factors are s-independent.

Calculations of the impact factors in the Born approximation[1] are standard [37]. They are obtained by assuming the collinear approximation at each $q\bar{q}\rho$-meson vertex. Projecting the (anti-) quark momenta on the Sudakov basis q'_1 and q'_2,

$$l_1 = z_1 q'_1 + l_{\perp 1} + z_1 r_\perp - \frac{(l_{\perp 1} + z_1 r_\perp)^2}{z_1 s}q'_2\,,$$
$$l'_1 = \bar{z}_1 q'_1 - l_{\perp 1} + \bar{z}_1 r_\perp - \frac{(-l_{\perp 1} + \bar{z}_1 r_\perp)^2}{\bar{z}_1 s}q'_2\,,$$
$$l_2 = z_2 q'_2 + l_{\perp 2} - z_2 r_\perp - \frac{(l_{\perp 2} - z_2 r_\perp)^2}{z_2 s}q'_1\,,$$
$$l'_2 = \bar{z}_2 q'_2 - l_{\perp 2} - \bar{z}_2 r_\perp - \frac{(-l_{\perp 2} - \bar{z}_2 r_\perp)^2}{\bar{z}_2 s}q'_1\,, \tag{13}$$

we put the relative momentum $l_{i\perp}$ to zero. For longitudinally polarized photons the impact factor reads

$$\mathcal{J}^{\gamma^*_{\rm L}(q_i)\to\rho_{\rm L}(k_i)}(\underline{k},\underline{r}-\underline{k})$$
$$= 8\pi^2\alpha_{\rm s}\frac{e}{\sqrt{2}}\frac{\delta^{ab}}{2N_c}Q_i f_\rho\alpha(k_i)\int_0^1\mathrm{d}z_i\,z_i\bar{z}_i\phi(z_i)\mathrm{P_P}(z_i,\underline{k},\underline{r},\mu_i)\,, \tag{14}$$

where the expression

$$\mathrm{P_P}(z_i,\underline{k},\underline{r},\mu_i) = \frac{1}{z_i^2\underline{r}^2+\mu_i^2} + \frac{1}{\bar{z}_i^2\underline{r}^2+\mu_i^2} - \frac{1}{(z_i\underline{r}-\underline{k})^2+\mu_i^2}$$
$$-\frac{1}{(\bar{z}_i\underline{r}-\underline{k})^2+\mu_i^2} \tag{15}$$

---

[1] Now, the forward impact factor of the $\gamma^*_{\rm L}(Q^2)\to\rho^0_{\rm L}$ transition has been calculated at the next-to-leading order accuracy in [38].

originates from the impact factor of quark pair production from a longitudinally polarized photon.

For transversally polarized photons, one obtains

$$\begin{aligned}&\mathcal{J}^{\gamma^*_{\mathrm{T}}(q_i)\to\rho_{\mathrm{L}}(k_i)}(\underline{k},\underline{r}-\underline{k})\\&=4\pi^2\alpha_{\mathrm{s}}\frac{e}{\sqrt{2}}\frac{\delta^{ab}}{2N_c}f_\rho\alpha(k_i)\\&\quad\times\int_0^1\mathrm{d}z_i\,(z_i-\bar{z}_i)\phi(z_i)\underline{\epsilon}\cdot\underline{\mathrm{Q}}(z_i,\underline{k},\underline{r},\mu_i)\,,\end{aligned}\tag{16}$$

where

$$\begin{aligned}\underline{\mathrm{Q}}(z_i,\underline{k},\underline{r},\mu_i)=&\frac{z_i\underline{r}}{z_i^2\underline{r}^2+\mu_i^2}-\frac{\bar{z}_i\underline{r}}{\bar{z}_i^2\underline{r}^2+\mu_i^2}+\frac{\underline{k}-z_i\underline{r}}{(z_i\underline{r}-\underline{k})^2+\mu_i^2}\\&-\frac{\underline{k}-\bar{z}_i\underline{r}}{(\bar{z}_i\underline{r}-\underline{k})^2+\mu_i^2}\end{aligned}\tag{17}$$

is proportional to the impact factor of quark pair production from a transversally polarized photon.

In the formulae (15) and (17) and for the rest of the paper, we denote $\mu_i^2=Q_i^2z_i\bar{z}_i+m^2$, where m is the quark mass. The limit $m\to0$ is regular, and we will restrict ourselves to the light quark case, thus taking $m=0$. Both impact factor (15) and (17) vanish when $\underline{k}\to0$ or $\underline{r}-\underline{k}\to0$ due to QCD gauge invariance.

In the formulae (14) and (16), ϕ is the distribution amplitude of the produced longitudinally polarized ρ^0-mesons. For the case with quark q of one flavor it is defined (see, e.g. [39]) by the matrix element of the non-local, gauge invariant correlator of quark fields on the light cone

$$\langle0|\bar{q}(x)\gamma^\mu q(-x)|\rho_{\mathrm{L}}(p)=\bar{q}q\rangle=f_\rho p^\mu\int_0^1\mathrm{d}z\,\mathrm{e}^{\mathrm{i}(2z-1)(px)}\phi(z)\,,\tag{18}$$

where the coupling constant is $f_\rho=216\,\mathrm{MeV}$, and where the gauge links are omitted to simplify the notation. ϕ is normalized to unity. The amplitudes for the production of ρ^0's are obtained by noting that $|\rho^0\rangle=1/\sqrt{2}(|\bar{u}u\rangle-|\bar{d}d\rangle)$.

Note that (18) corresponds to the leading twist collinear distribution amplitude. Such an object can be used strictly speaking for asymptotically large Q^2. In the phenomenological application of Sects. 4.2 and 5.3, in order to get measurable cross-sections, the dramatic decrease of the amplitudes with increase of Q_i^2, combined with the experimental conditions of the ILC project, requires rather low values of Q_i^2 (of the order of $1\,\mathrm{GeV}^2$), for which subleading twist contributions could be significant. This can be taken into account within a more phenomenological approach that incorporates an intrinsic k_{T} quark distribution and that goes beyond standard QCD collinear factorization [40, 41]. In the present paper we do not consider these effects and adhere to the collinear QCD factorization.

Let us label the amplitudes for the scattering process (3) through the polarization of the incoming virtual photons as $\mathcal{M}_{\lambda_1\lambda_2}$. They can be calculated using (12) and (14)–(17) supplemented by the choice of the transverse polarization vectors of the photons,

$$\underline{\epsilon}^{\pm}=\frac{1}{\sqrt{2}}(\mp1,-\mathrm{i})\tag{19}$$

and the longitudinal polarization vectors (7). For the case $\lambda_1=\lambda_2=0$:

$$\begin{aligned}\mathcal{M}_{00}=&\,\mathrm{i}sCQ_1Q_2\\&\times\int_0^1\mathrm{d}z_1\,\mathrm{d}z_2\,z_1\bar{z}_1\phi(z_1)z_2\bar{z}_2\phi(z_2)\mathrm{M}_{00}(z_1,z_2)\,,\end{aligned}\tag{20}$$

with

$$\begin{aligned}\mathrm{M}_{00}(z_1,z_2)=\int\frac{\mathrm{d}^2\underline{k}}{\underline{k}^2(\underline{r}-\underline{k})^2}&\mathrm{P_P}(z_1,\underline{k},\underline{r},\mu_1)\\&\times\mathrm{P_P}(z_2,-\underline{k},-\underline{r},\mu_2)\,;\end{aligned}\tag{21}$$

for the case $\lambda_2=+,-$:

$$\begin{aligned}\mathcal{M}_{0\lambda_2}=&\,\mathrm{i}s\frac{C}{2}Q_1\\&\times\int_0^1\mathrm{d}z_1\,\mathrm{d}z_2\,z_1\bar{z}_1\phi(z_1)(z_2-\bar{z}_2)\phi(z_2)\mathrm{M}_{0\lambda_2}(z_1,z_2)\,,\end{aligned}\tag{22}$$

with

$$\begin{aligned}\mathrm{M}_{0\lambda_2}(z_1,z_2)=\int\frac{\mathrm{d}^2\underline{k}}{\underline{k}^2(\underline{r}-\underline{k})^2}&\mathrm{P_P}(z_1,\underline{k},\underline{r},\mu_1)\\&\times\underline{\mathrm{Q}}(z_2,-\underline{k},-\underline{r},\mu_2)\cdot\underline{\epsilon}^{\lambda_2}\,;\end{aligned}\tag{23}$$

for the case $\lambda_1=+,-$:

$$\begin{aligned}\mathcal{M}_{\lambda_10}=&\,\mathrm{i}s\frac{C}{2}Q_2\\&\times\int_0^1\mathrm{d}z_1\,\mathrm{d}z_2\,(z_1-\bar{z}_1)\phi(z_1)z_2\bar{z}_2\phi(z_2)\mathrm{M}_{\lambda_10}(z_1,z_2)\,,\end{aligned}\tag{24}$$

with

$$\begin{aligned}\mathrm{M}_{\lambda_10}(z_1,z_2)=\int\frac{\mathrm{d}^2\underline{k}}{\underline{k}^2(\underline{r}-\underline{k})^2}&\underline{\mathrm{Q}}(z_1,\underline{k},\underline{r},\mu_1)\cdot\underline{\epsilon}^{\lambda_1}\\&\times\mathrm{P_P}(z_2,-\underline{k},-\underline{r},\mu_2)\,.\end{aligned}\tag{25}$$

and for the case $\lambda_1=+,-$, $\lambda_2=+,-$:

$$\begin{aligned}\mathcal{M}_{\lambda_1\lambda_2}=\mathrm{i}s\frac{C}{4}\int_0^1&\mathrm{d}z_1\,\mathrm{d}z_2\,(z_1-\bar{z}_1)\phi(z_1)(z_2-\bar{z}_2)\phi(z_2)\\&\times\mathrm{M}_{\lambda_1\lambda_2}(z_1,z_2)\,,\end{aligned}\tag{26}$$

with

$$\begin{aligned}\mathrm{M}_{\lambda_1\lambda_2}(z_1,z_2)=\int\frac{\mathrm{d}^2\underline{k}}{\underline{k}^2(\underline{r}-\underline{k})^2}&\underline{\mathrm{Q}}(z_1,\underline{k},\underline{r},\mu_1)\cdot\underline{\epsilon}^{\lambda_1(1)}\\&\times\underline{\mathrm{Q}}(z_2,-\underline{k},-\underline{r},\mu_2)\cdot\underline{\epsilon}^{\lambda_2(2)}\,.\end{aligned}\tag{27}$$

Here and in the rest of this paper, we denote $C=2\pi\frac{N_c^2-1}{N_c^2}\times\alpha_{\mathrm{s}}^2\alpha_{\mathrm{em}}f_\rho^2$. In terms of the above amplitudes, the corresponding differential cross-sections can be expressed in the large s limit (neglecting terms of order Q_i^2/s) as

$$\frac{\mathrm{d}\sigma^{\gamma^*_{\lambda_1}\gamma^*_{\lambda_2}\to\rho^0_{\mathrm{L}}\rho^0_{\mathrm{L}}}}{\mathrm{d}t}=\frac{|\mathcal{M}_{\lambda_1\lambda_2}|^2}{16\pi s^2}\,,\tag{28}$$

and it does not depend on s.

4 Non-forward Born order differential cross-section for $\gamma^*_{\mathrm{L,T}}\gamma^*_{\mathrm{L,T}} \to \rho^0_{\mathrm{L}}\rho^0_{\mathrm{L}}$

4.1 Analytical results for $k_\perp$-integrated amplitude $M_{\lambda_1\lambda_2}$

In this section we summarize the results for the amplitudes $M_{\lambda_1\lambda_2}$ obtained after performing analytically the $k_\perp$ integrals. Such analytic expressions give us the effective possibility of studying various kinematical limits in the variables Q_1^2, Q_2^2 and t. The $k_\perp$ integrations were done using the method of [22], which exploits in an efficient way the scaling properties of integrals appearing in conformal field theories. The generic $k_\perp$ integral involves an integrand that corresponds to a box diagram with two distinct massive propagators and two massless propagators. Because of that, the $k_\perp$ integrations result in long and complicate expressions. Thus, we discuss below only the general structure of the results and we relegate all technical details of $k_\perp$ integrations to the appendix.

In the transverse–transverse (TT) case, the amplitude can be expressed in terms of two projection operators in the transverse plane as follows:

$$\mathrm{M}_{\lambda_1\lambda_2}(z_1,z_2) = \left[a(\underline{r};Q_1,Q_2;z_1,z_2)\left(\delta^{ij} - \frac{r^i r^j}{r^2}\right) + b(\underline{r};Q_1,Q_2;z_1,z_2)\frac{r^i r^j}{r^2}\right]\epsilon_i^{\lambda_1}\epsilon_j^{\lambda_2}\,, \tag{29}$$

where we denote $\underline{r}^2 = r^2$.

Combining (26) and (29), and using $|M_{++}|^2 = |M_{--}|^2$, one gets in the case of two photons with the same polarization

$$\begin{aligned}|\mathcal{M}_{++}|^2 &= |\mathcal{M}_{--}|^2\\ &= s^2\frac{C^2}{64}\left|\int_0^1 \mathrm{d}z_1\,\mathrm{d}z_2\,(z_1-\bar{z}_1)\phi(z_1)(z_2-\bar{z}_2)\phi(z_2)\right.\\ &\quad\left.\times\left(b(\underline{r};Q_1,Q_2;z_1,z_2) - a(\underline{r};Q_1,Q_2;z_1,z_2)\right)\right|^2,\end{aligned} \tag{30}$$

and analogously for different polarizations:

$$\begin{aligned}|\mathcal{M}_{+-}|^2 &= s^2\frac{C^2}{64}\\ &\quad\times\left|\int_0^1 \mathrm{d}z_1\,\mathrm{d}z_2\,(z_1-\bar{z}_1)\phi(z_1)(z_2-\bar{z}_2)\phi(z_2)\right.\\ &\quad\left.\times\left(b(\underline{r};Q_1,Q_2;z_1,z_2) + a(\underline{r};Q_1,Q_2;z_1,z_2)\right)\right|^2.\end{aligned} \tag{31}$$

For the longitudinal–transverse (LT) case, restoring the dependency over all variables, one defines from (23) and (25) the scalar function f,

$$\mathrm{M}_{0\lambda}(\underline{r};Q_1,Q_2;z_1,z_2) = f(\underline{r};Q_1,Q_2;z_1,z_2)\,\underline{r}\cdot\underline{\epsilon}^{\lambda}\,, \tag{32}$$

or equivalently

$$\mathrm{M}_{\lambda 0}(\underline{r};Q_1,Q_2;z_1,z_2) = f(\underline{r};Q_2,Q_1;z_2,z_1)\,\underline{r}\cdot\underline{\epsilon}^{\lambda}\,, \tag{33}$$

which leads to

$$\begin{aligned}|\mathcal{M}_{0+}|^2 &= |\mathcal{M}_{0-}|^2\\ &= s^2\frac{C^2}{8}Q_1^2\underline{r}^2\left|\int_0^1 \mathrm{d}z_1\,\mathrm{d}z_2\,z_1\bar{z}_1\phi(z_1)(z_2-\bar{z}_2)\phi(z_2)\right.\\ &\quad\left.\times f(\underline{r};Q_1,Q_2;z_1,z_2)\right|^2.\end{aligned} \tag{34}$$

and analogously for the transverse–longitudinal (TL) case,

$$\begin{aligned}|\mathcal{M}_{+0}|^2 &= |\mathcal{M}_{-0}|^2\\ &= s^2\frac{C^2}{8}Q_2^2\underline{r}^2\left|\int_0^1 \mathrm{d}z_1\,\mathrm{d}z_2\,z_2\bar{z}_2\phi(z_2)(z_1-\bar{z}_1)\phi(z_1)\right.\\ &\quad\left.\times f(\underline{r};Q_2,Q_1;z_2,z_1)\right|^2.\end{aligned} \tag{35}$$

The expressions of $a(\underline{r};Q_1,Q_2;z_1,z_2)$, $b(\underline{r};Q_1,Q_2;z_1,z_2)$ and $f(\underline{r};Q_1,Q_2;z_1,z_2)$ presented as combinations of *finite* standard integrals are given in the appendix.

For the longitudinal–longitudinal (LL) case, it turned out [22] that (20) can be effectively replaced by $\widetilde{\mathrm{M}}(z_1,z_2)$, whose integral over $z_{1,2}$ with symmetrical DA gives the same result. $\widetilde{\mathrm{M}}(z_1,z_2)$ reads

$$\begin{aligned}\widetilde{\mathrm{M}}_{00}(z_1,z_2) = &-\left(\frac{1}{z_1^2\underline{r}^2+\mu_1^2} + \frac{1}{\bar{z}_1^2\underline{r}^2+\mu_1^2}\right)J_{3\mu_2}(z_2)\\ &-\left(\frac{1}{z_2^2\underline{r}^2+\mu_2^2} + \frac{1}{\bar{z}_2^2\underline{r}^2+\mu_2^2}\right)J_{3\mu_1}(z_1)\\ &+J_{4\mu_1\mu_2}(z_1,z_2) + J_{4\mu_1\mu_2}(\bar{z}_1,z_2)\,.\end{aligned} \tag{36}$$

$J_{3\mu}$ and $J_{4\mu_1\mu_2}$ are two dimensional integrals with respectively 3 propagators (1 massive) and 4 propagators (2 massive, with different masses); they are both IR and UV finite. Their expressions are given in the appendix.

Due to the collinear conformal subgroup $\mathrm{SL}(2,\mathrm{R})$ invariance [42], the ρ^0_{L} distribution amplitude has an expansion in terms of Gegenbauer polynomials of even order, which reads

$$\phi(z) = 6z(1-z)\left(1 + \sum_{n=1}^{\infty} a_{2n}C_{2n}^{3/2}(2z-1)\right). \tag{37}$$

Except for a short discussion in Sect. 5.3, we restrict ourselves to the asymptotical distribution amplitude corresponding to $a_{2n} = 0$.

To complete the evaluation of the amplitude $\mathcal{M}$, one needs to integrate over the quark momentum fractions z_1 and z_2 in the ρ mesons. For arbitrary values of t, it seems not possible to perform the z_1 and z_2 integrations analytically. We thus do them numerically. We observe the absence of the end-point singularity when $z_{1(2)} \to 0$ or $z_{1(2)} \to 1$. Indeed, for the longitudinal polarizations involving P_P as defined in (15), the z divergency of types $1/z$ and

$1/(1-z)$ is compensated by the $z\bar{z}$ factor when $z \to 0, 1$, while for transverse polarizations, involving $\underline{Q}$ as defined in (17), there is no singularity, since $\underline{Q}$ is itself regular.

For the special case $t = t_{\min}$ (where only the LL amplitude is non-vanishing), which will be useful in the discussion of Sects. 4.2 and 5.3, the integration over z_i can be performed analytically, with the result [22]

$$\begin{aligned}\mathcal{M}_{00} = -\mathrm{i}s\frac{N_c^2-1}{N_c^2}\alpha_{\rm s}^2\alpha_{\rm em}f_\rho^2\frac{9\pi^2}{2}\frac{1}{Q_1^2Q_2^2}\Bigg[&6\left(R+\frac{1}{R}\right)\ln^2 R \\ &+12\left(R-\frac{1}{R}\right)\ln R+12\left(R+\frac{1}{R}\right) \\ &+\left(3R^2+2+\frac{3}{R^2}\right)\big(\ln(1-R)\ln^2 R-\ln(R+1)\ln^2 R \\ &-2\mathrm{Li}_2(-R)\ln R+2\mathrm{Li}_2(R)\ln R \\ &+2\mathrm{Li}_3(-R)-2\mathrm{Li}_3(R)\big)\Bigg]\,, \qquad (38)\end{aligned}$$

where $R = Q_1/Q_2$. When $Q_1 = Q_2$, (38) simplifies to

$$\mathcal{M}_{00} = \mathrm{i}s\frac{N_c^2-1}{N_c^2}\alpha_{\rm s}^2\alpha_{\rm em}f_\rho^2\frac{9\pi^2}{Q^4}(14\zeta(3)-12)\,. \qquad (39)$$

4.2 Results for differential cross-section

The formulae for $\mathrm{M}_{\lambda_1\lambda_2}$ obtained in Sect. 4 permit us to evaluate the magnitudes of cross-sections (28) of the diffractive double rho production for different helicities of the virtual photons. In our estimates we use as a strong coupling constant the three-loop running $\alpha_{\rm s}(Q_1Q_2)$ with $\Lambda^{(4)}_{\overline{\rm MS}} = 305$ MeV (see, e.g. [43]).[2]

In Fig. 5 we display the t-dependence of the different $\gamma^*_{\rm L,T}\gamma^*_{\rm L,T} \to \rho^0_{\rm L}\rho^0_{\rm L}$ differential cross-sections for various values of $Q = Q_1 = Q_2$.

We first note the strong decrease of all the cross-sections when $Q^2_{1,2}$ increase. For LL, this follows from an obvious dimensional analysis, since

$$\mathcal{M}_{\rm LL} \propto \frac{sf_\rho^2}{Q^4}$$

(for $Q_1 = Q_2 = Q$), in agreement with (39).

Secondly, all the differential cross-sections that involve at least one transverse photon vanish when $t = t_{\min}$. It is due to the vanishing of the function $\underline{Q}$ for $\underline{r} = 0$ (see (17)). Physically, this fact is related to the s-channel helicity conservation at $t = t_{\min}$. Indeed, since the t-channel gluons carry non-sense polarizations, helicity conservation occurs separately in each impact factor.

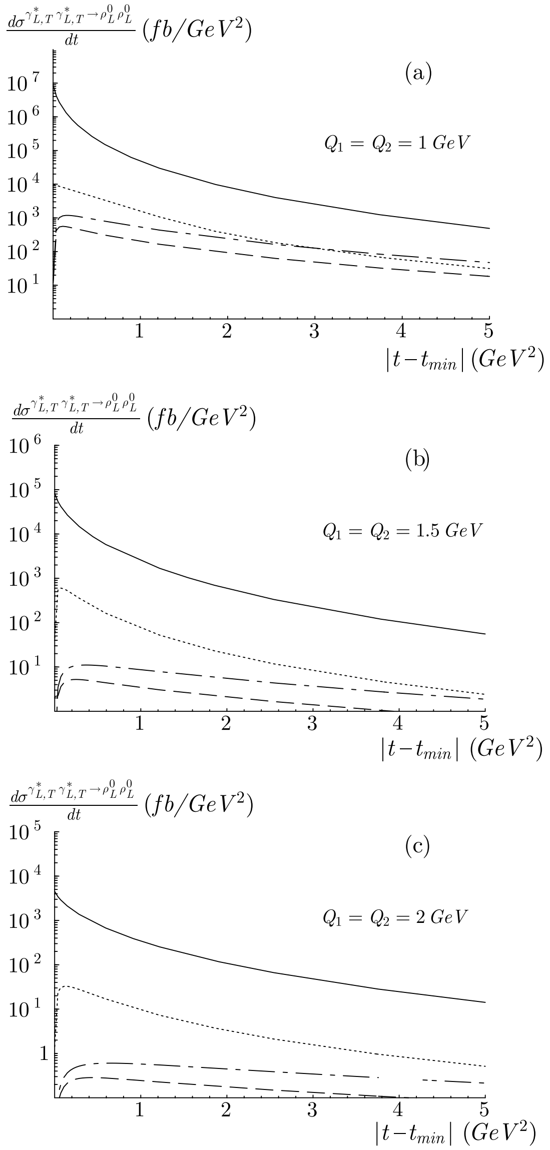

Fig. 5. Differential cross-sections for the process $\gamma^*_{\rm L,T}\gamma^*_{\rm L,T} \to \rho^0_{\rm L}\rho^0_{\rm L}$. The *solid curve* corresponds to the $\gamma^*_{\rm L}\gamma^*_{\rm L}$ mode, the *dotted one* to the $\gamma^*_{\rm L}\gamma^*_{\rm T}$ mode, the *dashed* and the *dashed-dotted ones* to the $\gamma^*_{\rm T}\gamma^*_{\rm T'}$ modes with respectively the same $\rm T = T'$ and different $\rm T \neq T'$ transverse polarizations. The different figures **a**–**c** correspond to different values of $Q_1 = Q_2$

In Fig. 6, we show the shape of the integrands $\overline{\mathrm{M}}_{\lambda_1,\lambda_2}$ of the various amplitudes $\mathcal{M}_{\lambda_1\lambda_2}$ as a function of z_1 and z_2, as they appear in formulas (22), (24) and (26):

$$\overline{\mathrm{M}}_{00} = z_1\bar{z}_1\phi(z_1)z_2\bar{z}_2\phi(z_2)\mathrm{M}_{00}(z_1,z_2)\,, \qquad (40)$$

and for $\lambda_i = +, -$

$$\overline{\mathrm{M}}_{\lambda_1 0} = (z_1-\bar{z}_1)\phi(z_1)z_2\bar{z}_2\phi(z_2)\mathrm{M}_{\lambda_1 0}(z_1,z_2)\,, \qquad (41)$$

$$\overline{\mathrm{M}}_{\lambda_1\lambda_2} = (z_1-\bar{z}_1)\phi(z_1)(z_2-\bar{z}_2)\phi(z_2)\mathrm{M}_{\lambda_1\lambda_2}(z_1,z_2)\,. \qquad (42)$$

---

[2] Running of $\alpha_{\rm s}$ is in principle a subleading effect with respect to our treatment. Nevertheless, numerically, as we discuss in Sect. 5.3, the dependence of our predictions for the rates in e^+e^- scattering on the choice of $\alpha_{\rm s}$ is negligible at Born order, but it is more subtle when LO BFKL corrections are taken into account.

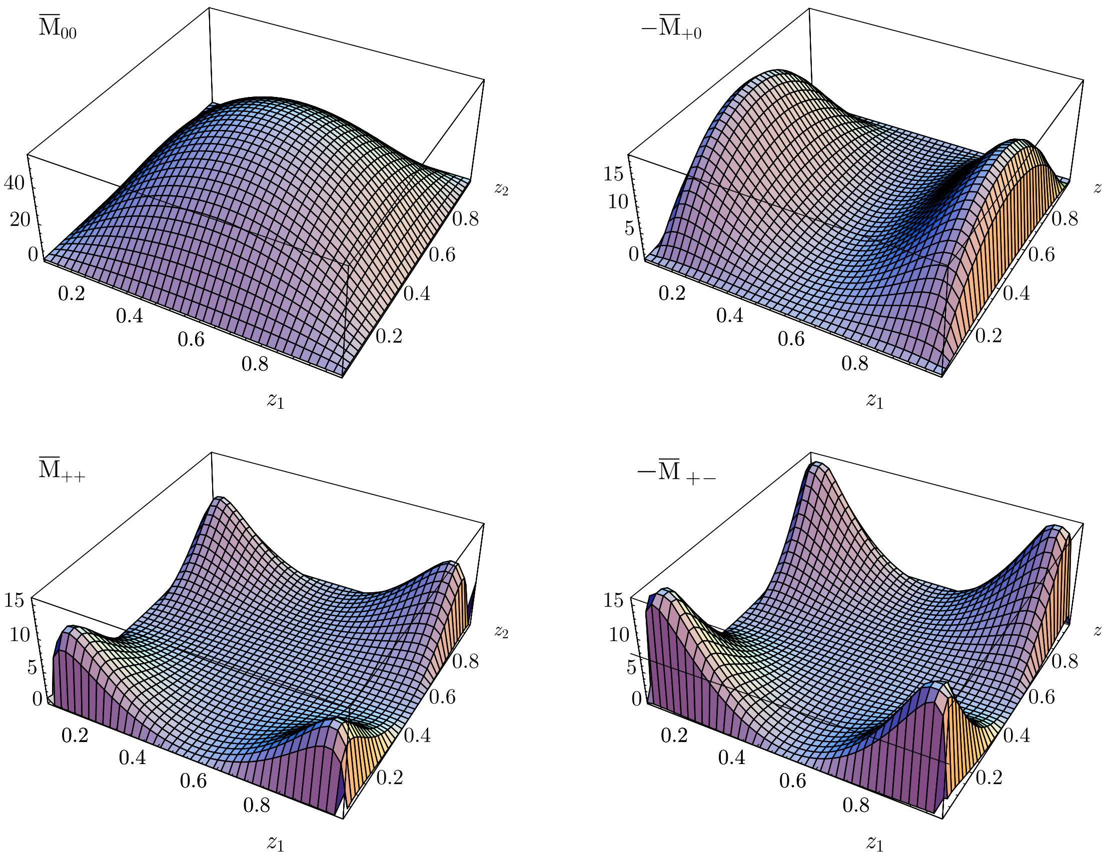

Fig. 6. Shape of the amplitudes $\overline{\mathrm{M}}_{00}$, $-\overline{\mathrm{M}}_{+0}$, $\overline{\mathrm{M}}_{++}$, $-\overline{\mathrm{M}}_{+-}$ as functions of z_1 and z_2, for $-t = 0.16\,\mathrm{GeV}^2$ and $Q_1 = Q_2 = 1\,\mathrm{GeV}$

$\mathrm{M}_{\lambda_1\lambda_2}(z_1, z_2)$ is symmetric under $(z_i \leftrightarrow \bar{z}_i)$ for longitudinal polarization, $\lambda_i = 0$ (cf. (15)) and antisymmetric under $(z_i \leftrightarrow \bar{z}_i)$ for transverse polarization, $\lambda_i = +, -$ (cf. (17)); thus the factors $z_i\bar{z}_i$ for $\lambda_i = 0$ and $z_i - \bar{z}_i$ for $\lambda_i = +, -$ ensure the symmetry of $\overline{\mathrm{M}}_{\lambda_1\lambda_2}$ under $(z_i \leftrightarrow \bar{z}_i)$ as we can see on Fig. 6. Because of the ρ^0_{L} meson distribution amplitudes $\phi(z_i)$, $\overline{\mathrm{M}}_{\lambda_1\lambda_2}(z_1, z_2)$ vanishes for any polarization in the end-point region. Consequently the case of transverse polarization vanishes in the central region $z_i = \bar{z}_i = 1/2$ and also in the end-point region z_i close to 0 or 1, so that it restricts the available z_i phase space and reduces the resulting differential cross-section, in agreement with the dominance of longitudinal photons (helicity conservation) in the process $\gamma^*_{\mathrm{L,T}}\gamma^*_{\mathrm{L,T}} \to \rho^0_{\mathrm{L}}\rho^0_{\mathrm{L}}$.

The amplitude involving at least one transverse photon has a maximum at low $-t$ value with respect to Q_1Q_2. Figure 6 corresponds to $-t = 0.16\,\mathrm{GeV}^2$, which is a typical value for the region where the cross-sections with transverse photons in Fig. 5 are maximal.

A peculiarly characteristic shape appears in the amplitudes with two transverse photons, as shown in the bottom panels of Fig. 6. When the value of t changes towards $t_{\min}$, the peaks become very narrow, as shown in the left panel in Fig. 7 for $\overline{\mathrm{M}}_{+-}$. For t very close to $t_{\min}$ they are practically

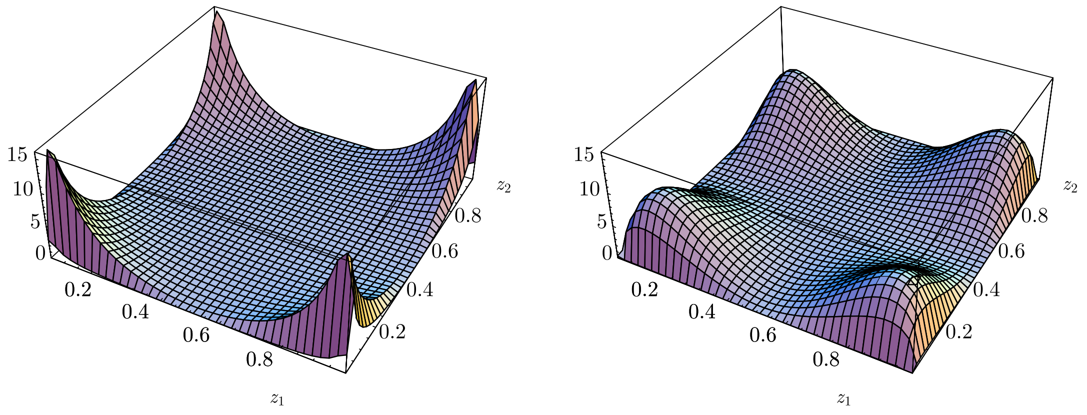

Fig. 7. Shape of the amplitude $-\overline{\mathrm{M}}_{+-}$, for $-t = 0.01\,\mathrm{GeV}^2$ (*left*) and $-t = 0.8\,\mathrm{GeV}^2$ (*right*), with $Q_1 = Q_2 = 1\,\mathrm{GeV}$

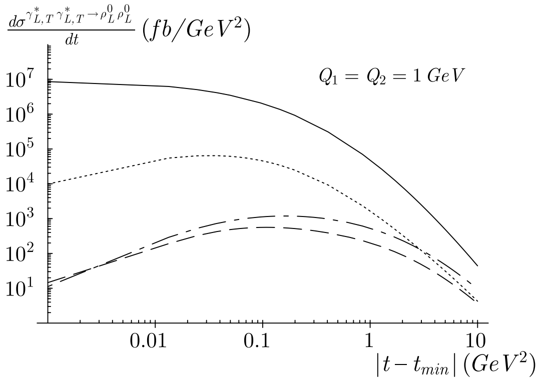

Fig. 8. Differential cross-sections for the process $\gamma^*_{\mathrm{L,T}}\gamma^*_{\mathrm{L,T}} \to \rho^0_{\mathrm{L}}\rho^0_{\mathrm{L}}$, for small value of t. The *solid curve* corresponds to the $\gamma^*_{\mathrm{L}}\gamma^*_{\mathrm{L}}$ mode, the *dotted one* to the $\gamma^*_{\mathrm{L}}\gamma^*_{\mathrm{T}}$ mode, the *dashed* and the *dashed-dotted ones* to the $\gamma^*_{\mathrm{T}}\gamma^*_{\mathrm{T'}}$ modes with respectively the same $\mathrm{T} = \mathrm{T'}$ and different $\mathrm{T} \neq \mathrm{T'}$ transverse polarizations, for $Q_1 = Q_2 = 1$ GeV

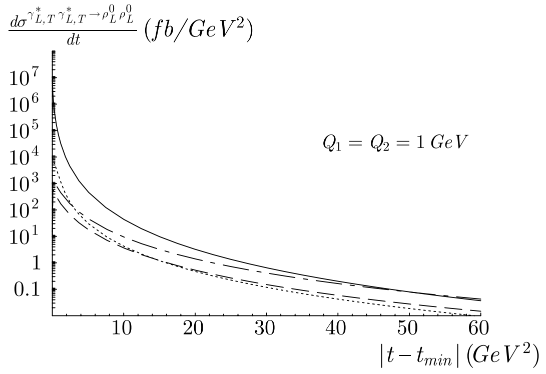

Fig. 9. Differential cross-sections for the process $\gamma^*_{\mathrm{L,T}}\gamma^*_{\mathrm{L,T}} \to \rho^0_{\mathrm{L}}\rho^0_{\mathrm{L}}$, up to asymptotically large t. The *solid curve* corresponds to the $\gamma^*_{\mathrm{L}}\gamma^*_{\mathrm{L}}$ mode, the *dotted one* to the $\gamma^*_{\mathrm{L}}\gamma^*_{\mathrm{T}}$ mode, the *dashed* and the *dashed-dotted ones* to the $\gamma^*_{\mathrm{T}}\gamma^*_{\mathrm{T'}}$ modes with respectively the same $\mathrm{T} = \mathrm{T'}$ and different $\mathrm{T} \neq \mathrm{T'}$ transverse polarizations, for $Q_1 = Q_2 = 1$ GeV

concentrated only on the boundary, which leads to the vanishing of the amplitude. On the other hand, when the value of t increases and leaves the maximum of the cross-sections, the peaks in Fig. 6 decrease and spread, as shown for $\overline{\mathrm{M}}_{+-}$ in the right panel of Fig. 7.

In the case of LT polarizations, the shape of the amplitude $\overline{\mathrm{M}}_{+0}$, which contains only one factor $(z_i - \bar{z}_i)$, is shown in the right upper panel of Fig. 6. Comparison with the upper left panel of Fig. 6, showing the shape of the $\overline{\mathrm{M}}_{00}$ amplitude, leads to the conclusion that $\overline{\mathrm{M}}_{+0}$ shares some properties with $\overline{\mathrm{M}}_{+-}$ and $\overline{\mathrm{M}}_{00}$. In particular, the presence of a transverse polarization leads to the vanishing of $\overline{\mathrm{M}}_{+0}$ at $t = t_{\min}$. On the other hand, the presence of longitudinal polarization increases the cross-section at small values of t. As a consequence of the competition of these two mechanisms, the maximum of the cross-section determined by $\overline{\mathrm{M}}_{+0}$ is located closer to $t_{\min}$ than in the case of the cross-section given by $\overline{\mathrm{M}}_{+-}$. This is illustrated in Fig. 8, which shows the t-dependence of the various differential cross-sections in log–log scale.

Third, in Fig. 9, we display the t-dependence of the $\gamma^*_{\mathrm{L,T}}\gamma^*_{\mathrm{L,T}} \to \rho^0_{\mathrm{L}}\rho^0_{\mathrm{L}}$ differential cross-sections for $Q = Q_1 = Q_2 = 1$ GeV up to values of $-t$ much larger than the photon virtualities Q_i, where t plays the role of the dominant hard scale in our process. Of course, in such a kinematical region the cross-sections are strongly suppressed in comparison with the small t one. Nevertheless, Fig. 9 illustrates the expected fact that the hierarchy of cross-sections is different in two regions: at large t, the $\gamma^*_{\mathrm{T}}\gamma^*_{\mathrm{T}} \to \rho^0_{\mathrm{L}}\rho^0_{\mathrm{L}}$ cross-section dominates over the one of $\gamma^*_{\mathrm{L}}\gamma^*_{\mathrm{L}} \to \rho^0_{\mathrm{L}}\rho^0_{\mathrm{L}}$, which is the dominant cross-section at small t, since the virtual photons are almost on shell with respect to the large scale given by t.

To conclude this subsection, we note that all the above cross-sections are strongly peaked in the forward cone. The phenomenological predictions obtained in the region of the forward cone will practically dictate the general trends of the integrated cross-sections. This fact is less dangerous than for the real photon case, since the virtual photon is not in the direction of the beam, and thus the outgoing ρ mesons can be tagged. The only difficulty has to do with the tagging of the outgoing lepton, since the cross-section is dominated by small (hard) values of $Q^2_{1,2}$. In this section we did not modify cross-sections by taking into account the virtual photon fluxes, which would amplify both the dominance of the small Q^2 region as well as the small y_i domain, characteristic for very forward outgoing leptons. This is discussed in Sect. 5. In particular, it will be shown that the differential cross-sections are experimentally visible and seem to be sufficient for the t-dependence to be measured up to a few GeV^2.

Note also that at this level of calculation there is no s-dependence of the cross-section. It will appear after taking into account triggering effects and/or BFKL evolution.

4.3 Quark exchange contribution to the cross-section

The process (3) described above involves gluon exchanges that dominate at high energies. However, at lower energy, the process can be described by double quark exchange. This was investigated in [25], in the case $t = t_{\min}$. Figure 10 shows in particular the diagrams that contribute to the amplitude M_H (see Fig. 2) for the process $\gamma^*_{\mathrm{L}}(q_1)\gamma^*_{\mathrm{L}}(q_2) \to \rho_{\mathrm{L}}(k_1)\rho_{\mathrm{L}}(k_2)$. Using (12) and (13) of [25] together with the asymptotical ρ^0_{L} distribution amplitude (37) one obtains the scattering amplitude for the photons longitudinally polarized:

$$\mathcal{M}_{00}^{q\bar{q}} = -40\pi^2 \frac{N_c^2-1}{N_c^2}\frac{\alpha_{\mathrm{s}}\alpha_{\mathrm{em}} f_\rho^2}{s} \times \left[1+\frac{\left(1+\frac{Q_1^2}{s}+2\frac{Q_1^2}{s}\frac{\ln\frac{Q_1^2}{s}}{1-\frac{Q_1^2}{s}}\right)\left(1+\frac{Q_2^2}{s}+2\frac{Q_2^2}{s}\frac{\ln\frac{Q_2^2}{s}}{1-\frac{Q_2^2}{s}}\right)}{\left(1-\frac{Q_1^2}{s}\right)\left(1-\frac{Q_2^2}{s}\right)}\right] \tag{43}$$

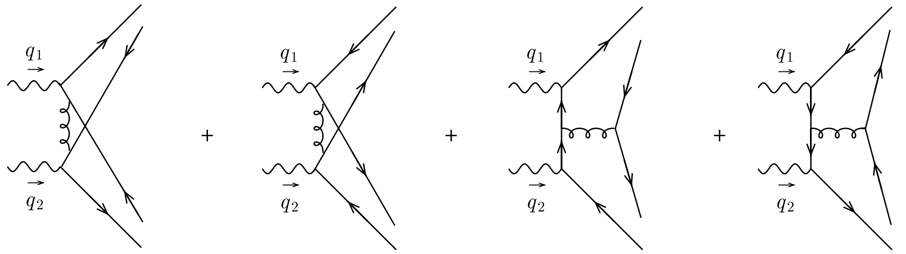

Fig. 10. Feynman diagrams contributing to M_H in the case of longitudinally polarized virtual photons

and for the transversally polarized photons

$$\begin{aligned}\mathcal{M}^{q\bar{q}}_{\mathrm{TT}} &= \mathcal{M}^{q\bar{q}}_{++} + \mathcal{M}^{q\bar{q}}_{--}\\ &= -40\pi^2 \frac{N_c^2-1}{N_c^2}\frac{\alpha_{\mathrm{s}}\alpha_{\mathrm{em}} f_\rho^2}{s}\\ &\quad\times \frac{\left(\frac{7}{2} + \frac{2\left(1+\frac{Q_1^2}{s}\right)\ln\frac{Q_1^2}{s}}{1-\frac{Q_1^2}{s}}\right)\left(\frac{7}{2} + \frac{2\left(1+\frac{Q_2^2}{s}\right)\ln\frac{Q_2^2}{s}}{1-\frac{Q_2^2}{s}}\right) - \frac{1}{4}}{\left(1-\frac{Q_1^2}{s}\right)\left(1-\frac{Q_2^2}{s}\right)}\,.\end{aligned} \tag{44}$$

In the large s limit, one respectively gets

$$\mathcal{M}^{q\bar{q}}_{00} \simeq -80\pi^2 \frac{N_c^2-1}{N_c^2}\frac{\alpha_{\mathrm{s}}\alpha_{\mathrm{em}} f_\rho^2}{Q_1 Q_2} \tag{45}$$

and

$$\begin{aligned}\mathcal{M}^{q\bar{q}}_{\mathrm{TT}} &\simeq -40\pi^2 \frac{N_c^2-1}{N_c^2}\frac{\alpha_{\mathrm{s}}\alpha_{\mathrm{em}} f_\rho^2}{s}\\ &\quad\times\left(4\ln\frac{Q_1^2}{s}\ln\frac{Q_2^2}{s} + 14\ln\frac{Q_1 Q_2}{s} + 12\right)\\ &= -40\pi^2 \frac{N_c^2-1}{N_c^2}\frac{\alpha_{\mathrm{s}}\alpha_{\mathrm{em}} f_\rho^2}{s}\\ &\quad\times\left(4\ln^2\frac{Q_1 Q_2}{s} + 14\ln\frac{Q_1 Q_2}{s} - 4\ln^2 Q_1/Q_2 + 12\right).\end{aligned} \tag{46}$$

Other amplitudes vanish at $t = t_{\mathrm{min}}$.

These expressions should be compared with the corresponding two gluon exchange contributions discussed in the previous sections. The LL amplitude is almost constant around $t = t_{\mathrm{min}}$ and given by (38).

The TT amplitude (29) behaves as

$$\mathcal{M}^{gg}_{\mathrm{TT}} \simeq -\mathrm{i}a\frac{\pi}{2}s\frac{N_c^2-1}{N_c^2}\alpha_{\mathrm{s}}^2\alpha_{\mathrm{em}} f_\rho^2 \frac{|t-t_{\mathrm{min}}|}{Q_1^3 Q_2^3}, \tag{47}$$

where the constant $a = 253.5$ is extracted from a numerical fit.

Equations (43)–(47) confirm the well known fact that in the Regge limit two gluon exchange dominates over double quark exchange. Indeed, comparison of (45) and (46) with (38) and (47) shows that the gluonic contributions are proportional to s (in agreement with the usual counting rule $s^{\Sigma\sigma_i - N + 1}$, where N is the number of t-channel exchanged particles of spin σ_i). In the case of longitudinally polarized photons, which does not vanish at t_{min}, and for the same photon virtualities $Q_1^2 = Q_2^2 = Q^2$, let us consider the ratio

$$\mathcal{R}_{\mathrm{LL}} = \frac{\mathcal{M}^{q\bar{q}}_{00}}{\mathcal{M}^{gg}_{00}} = \frac{32(Q_u^2 + Q_d^2)}{28\zeta(3) - 24}\frac{Q^2}{s\alpha_{\mathrm{s}}}\,. \tag{48}$$

For a typical value of $Q^2 = 1\,\mathrm{GeV}^2$, as soon as s ($\simeq s_{\gamma^*\gamma^*}$) is higher than $4\,\mathrm{GeV}^2$, this ratio is larger than unity, which at first sight seems to be always the case for ILC. Equation (38) would thus completely dominate with respect to (43), by several orders of magnitudes. In fact, $s_{\gamma^*\gamma^*}$ can reach such a low value as $4\,\mathrm{GeV}^2$, because of the outgoing energy carried by the outgoing leptons and the strong peak of the Weizsäcker–Williams fluxes at small γ^* energies. We discuss this effect in Sect. 5.3 at the level of the e^+e^- process, after performing the phase-space integration of the differential cross-section at t_{min}. It will be shown that nevertheless the quark contribution is really negligible in almost all the ILC phase space.

In the case of the two gluon contribution with transverse virtual photons, (47), which vanishes at $t = t_{\mathrm{min}}$, its dominance over the corresponding quark contribution (44) appears very rapidly when $|t - t_{\mathrm{min}}|$ starts to increase, and it persists in the whole essential region of the phase space (remember that (47) is peaked at $t - t_{\mathrm{min}} = k0.01\,\mathrm{GeV}^2$, where k is of order 1–10). This dominance will also be discussed in more detail in Sect. 5.3 at the level of the e^+e^- process.

5 Non-forward Born order cross-section for $e^+e^- \to e^+e^-\rho_{\mathrm{L}}^0\rho_{\mathrm{L}}^0$

5.1 Kinematical cuts for the phase-space integration

Our purpose is now to evaluate the cross-section of the process $e^+e^- \to e^+e^-\rho_{\mathrm{L}}^0\rho_{\mathrm{L}}^0$ in the planned experimental conditions of the International Linear Collider project [44]. For the detector part, we chose to focus on the Large Detector Concept [45], and we use the potential of the very forward region accessible through the electromagnetic calorimeter BeamCal, which may be installed around the beampipe at 3.65 m from the interaction point. The LDC is illustrated in Fig. 11.

The cross-section that takes into account all the kinematical constraints, which are explained below, is given by

$$\begin{aligned}\frac{\mathrm{d}\sigma^{e^+e^-\to e^+e^-\rho_{\mathrm{L}}\rho_{\mathrm{L}}}}{\mathrm{d}t} &= \int_{Q^2_{1\,\mathrm{min}}}^{Q^2_{1\,\mathrm{max}}}\mathrm{d}Q_1^2 \int_{Q^2_{2\,\mathrm{min}}}^{Q^2_{2\,\mathrm{max}}}\mathrm{d}Q_2^2 \int_{\epsilon}^{y_{\mathrm{max}}}\mathrm{d}y_1\\ &\quad\times\int_{\frac{Q_1 Q_2}{s y_1}}^{y_{\mathrm{max}}}\mathrm{d}y_2\,\frac{\mathrm{d}\sigma^{e^+e^-\to e^+e^-\rho_{\mathrm{L}}\rho_{\mathrm{L}}}}{\mathrm{d}t\,\mathrm{d}y_1\,\mathrm{d}y_2\,\mathrm{d}Q_1^2\,\mathrm{d}Q_2^2}\,,\end{aligned} \tag{49}$$

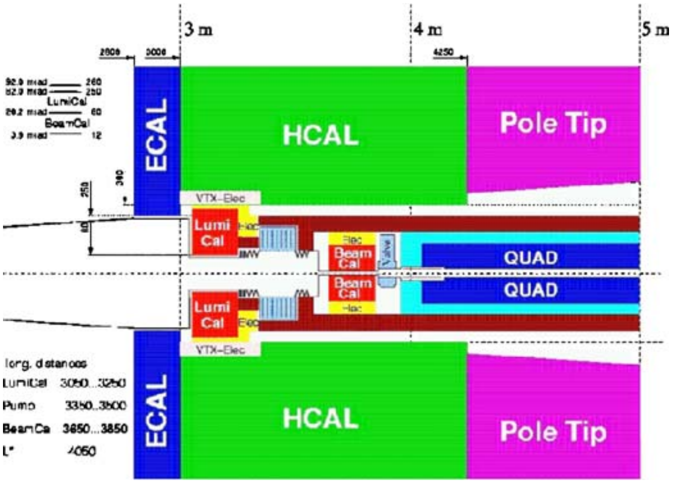

Fig. 11. The LDC project, with the BeamCal forward electromagnetic calorimeter

with $Q_{1\,\mathrm{min}} = 1\,\mathrm{GeV}$, $Q_{1\,\mathrm{max}} = 4\,\mathrm{GeV}$, $\epsilon = 10^{-6}$ and $y_{\mathrm{max}} = 0.6$.

The cross-section (49) can be evaluated combining the cross-section formulae (5) and (28) and the results of Sect. 4.2 for the helicity scattering amplitudes.

The important feature of the formula (49) is that the dominant contribution for the $e^+e^- \to e^+e^-\rho_L^0\rho_L^0$ process is strongly peaked at low Q_i. The integration over Q_i and y_i is peaked in the low y_i and Q_i phase-space region due to the presence in (5) of $1/(y_iQ_i^2)$ factors coming from the Weizsäcker–Williams fluxes and thus amplifies this effect. We show below that this dominant part of the phase space is accessible experimentally using the BeamCal calorimeter.

The integration domain in (49) is fixed by the following considerations. In the laboratory frame, which is also the center of mass system (CMS) for a linear collider, the standard expression for the momentum fractions with respect to the incoming leptons and for the virtualities of the bremsstrahlung photons are, respectively, given by

$$y_i = \frac{E - E_i' \cos^2(\theta_i/2)}{E}\,, \quad Q_i^2 = 4EE_i' \sin^2(\theta_i/2)\,, \quad (50)$$

where E is the energy of the beam, while E_i' and θ_i are, respectively, the energy and the scattering angle of the outgoing leptons. At ILC, the foreseen CMS energy is $\sqrt{s} = 2E = 500\,\mathrm{GeV}$. The experimental constraint coming from the minimal detection angle θ_{min} around the beampipe is given by $\theta_{\mathrm{max}} = \pi - \theta_{\mathrm{min}} > \theta_i > \theta_{\mathrm{min}}$ and leads to the following constraint on y_i:

$$y_i > f(Q_i) = 1 - \frac{Q_i^2}{s \tan^2(\theta_{\mathrm{min}}/2)}\,, \quad (51)$$

where the constraint on the upper bound of y_i coming from θ_{max} is completely negligible at this CMS energy.

The condition on the energy of the scattered lepton $E_{\mathrm{max}} > E_i' > E_{\mathrm{min}}$ results in

$$y_{i\,\mathrm{max}} = 1 - \frac{E_{\mathrm{min}}}{E} > y_i > 1 - \frac{E_{\mathrm{max}}}{E}\,. \quad (52)$$

Moreover, we impose $s_{\gamma^*\gamma^*} = y_1y_2s > cQ_1Q_2$ (where c is an arbitrary constant of the order 1), which is required by the Regge kinematics for which the impact representation is valid. In Sect. 5.3 we show that this constant c can be adjusted to choose bins of data for which also in the case of e^+e^- scattering the contribution with quark exchanges (discussed in Sect. 4.3) is completely negligible.

We arbitrarily choose Q_i to be bigger than 1 GeV as it provides the hard scale of the process, which legitimates the use of perturbation theory. $Q_{i\,\mathrm{max}}$ will be fixed to 4 GeV, since the various amplitudes involved are completely negligible for higher values of the virtualities Q_i (see Sect. 4.2). The constraints on $y_{i\,\mathrm{min}}$ discussed so far are summarized by the conditions

$$y_{1\,\mathrm{min}} = \max\left(f(Q_1), 1 - \frac{E_{\mathrm{max}}}{E}\right) \quad \text{and}$$
$$y_{2\,\mathrm{min}} = \max\left(f(Q_2), 1 - \frac{E_{\mathrm{max}}}{E}, \frac{cQ_1Q_2}{sy_1}\right). \quad (53)$$

Further simplifications of the conditions (53) can be done by taking into account that the only condition on the maximal value of energy detection of the scattered leptons comes from kinematics, i.e. $E_{\mathrm{max}} = E$, and accounting for some specific features of the planned detector.

The BeamCal calorimeter in the very forward region in principle allows one to detect particles down to 4 mrad.[3] More precisely, it measures an energy deposit for an angle between 4 mrad and 26 mrad. But this detector is also polluted by photon beamstrahlung, specially for very small angles (see Fig. 12). We assume a non-ambiguous identification for particles whose energies are bigger than 100 GeV. More precisely, the efficiency of detection of an electron depends on its energy and becomes less ambiguous when the energy increases. It is above 70% in the part of the phase space that dominates the cross-section (small y_i, corresponding to $E_i' \simeq E_i$). A precise evaluation of this efficiency would require to set up a Monte Carlo simulation for the beamstrahlung contribution, which is beyond the scope of this paper. This sets the maximal value of y_i to $y_{i\,\mathrm{max}} = 1 - \frac{E_{\mathrm{min}}}{E} = 0.6$ with $E_{\mathrm{min}} = 100\,\mathrm{GeV}$ and $E = 250\,\mathrm{GeV}$.

Such a big value of E_{min} can be considered as surprisingly high and could lead to a strong reduction of the allowed phase space. In principle, one could enlarge the phase space by taking into account particles whose energies E_i' are between 100 GeV and 20 GeV with angles θ_i bigger than 10 mrad (see Fig. 12), but the contribution of this domain is negligible (see Fig. 13), since the lower bound of y_i (see (53)) prevents us from reaching the small values of y_i and Q_i that give the dominant contribution to the cross-section. We safely neglect the contribution of this region of phase space and assume in the following that $E_{\mathrm{min}} = 100$ GeV and $\theta_{\mathrm{min}} = 4$ mrad.

---

[3] Note that in order to get access to any inclusive [17] or diffractive high s processes, one needs very small θ_{min}. To reach values of θ_{min} of a few mrads represents an important technological step, which was not feasible a few years ago.

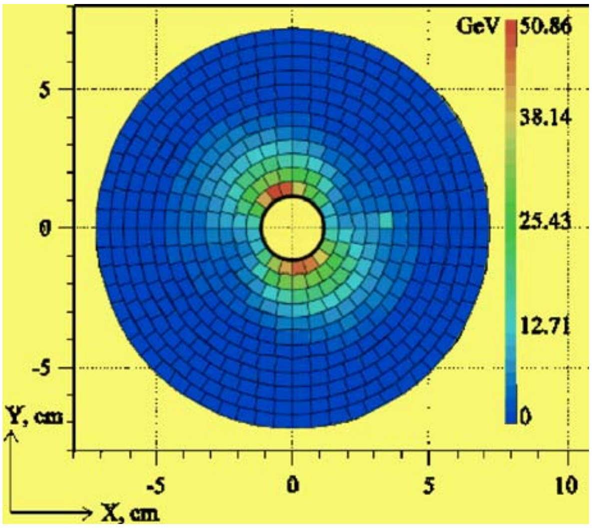

Fig. 12. Energy deposit in GeV in each cell of the BeamCal detector due to beamstrahlung

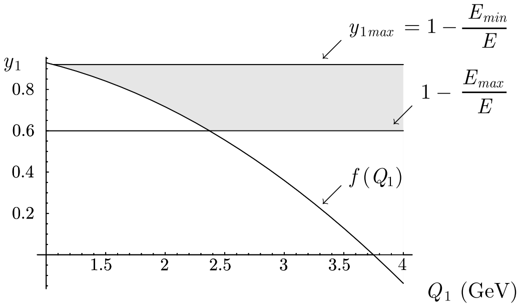

Fig. 13. y_1 integration domain for $\theta_{\min} = 10\,\mathrm{mrad}$, $E_{\min} = 20\,\mathrm{GeV}$ and $E_{\max} = 100\,\mathrm{GeV}$

Thus, with $\theta_{\min} = 4\,\mathrm{mrad}$ and $\sqrt{s} = 500\,\mathrm{GeV}$, we have $s\tan^2(\theta_{\min}/2) = 1\,\mathrm{GeV}^2$, which means that $f(Q) \le 0$ for $Q^2 \ge 1\,\mathrm{GeV}^2$. The relations (53), with $E_{\max} = E$, reduce to only one condition $y_{2\,\min} = \frac{Q_1 Q_2}{s y_1}$. This has to be supplemented numerically with the condition $y_{1\,\min} = \epsilon$, where ϵ is a numerical cut-off: although, because of the Regge limit condition, we have $y_1 > \frac{Q_1 Q_2}{s y_2} \ge \frac{Q_{1\,\min} Q_{2\,\min}}{s y_{2\,\max}} = 6.6 \times 10^{-6}$ which thus provides a natural lower cut-off for y_1, nevertheless we choose $\epsilon = 10^{-6}$ so that it is smaller than the smallest reachable value of y_1 but still non-zero. This cut-off has no practical effect, except for avoiding numerical instabilities in the integration code.

The above discussion justifies the various cuts in formula (49).

5.2 Background in the detector

BeamCal is an electromagnetic calorimeter that cannot distinguish charges of particles. Thus, it is important to check that the cross-sections of any other processes that could lead to final states that can be misidentified with the final state of the process $e^+e^- \to e^+e^-\rho_{\mathrm{L}}^0\rho_{\mathrm{L}}^0$ are suppressed. Indeed, the final state of the process $e^+e^- \to \gamma\gamma\rho_{\mathrm{L}}^0\rho_{\mathrm{L}}^0$, with photons of the same energy deposit in detector as outgoing leptons, cannot be distinguished with the final state of $e^+e^- \to e^+e^-\rho_{\mathrm{L}}^0\rho_{\mathrm{L}}^0$.

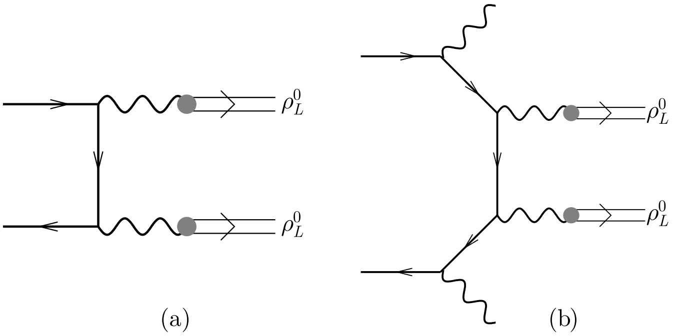

(a) (b)

Fig. 14. Example of Born order diagrams for the process $e^+e^- \to \rho_{\mathrm{L}}^0\rho_{\mathrm{L}}^0$ (**a**) and for the $e^+e^- \to \gamma\gamma\rho_{\mathrm{L}}^0\rho_{\mathrm{L}}^0$ process (**b**)

We shall argue that the process $e^+e^- \to \gamma\gamma\rho_{\mathrm{L}}^0\rho_{\mathrm{L}}^0$ leads to a cross-section that is negligible at ILC. Let us start with the process $e^+e^- \to \rho_{\mathrm{L}}^0\rho_{\mathrm{L}}^0$ illustrated in Fig. 14a, studied in [46, 47].

Its differential cross-section behaves typically like

$$\frac{\mathrm{d}\sigma}{\mathrm{d}t} \propto \frac{\alpha_{\mathrm{em}}^4 f_\rho^4}{s^2 m_\rho^4}\,, \tag{54}$$

with the virtualities of the photons propagators equal to m_ρ^2. More accurate expressions can be found in [47], if one identifies $g_{V\gamma} = f_\rho m_\rho$.

Now, when considering the competitor process $e^+e^- \to \gamma\gamma\rho_{\mathrm{L}}^0\rho_{\mathrm{L}}^0$, that is, adding two additional bremsstrahlung photons as in Fig. 14b, we get

$$\frac{\mathrm{d}\sigma^{e^+e^-\to\gamma\gamma\rho_{\mathrm{L}}\rho_{\mathrm{L}}}}{\mathrm{d}t\,\mathrm{d}y_1\,\mathrm{d}y_2\,\mathrm{d}Q_1^2\,\mathrm{d}Q_2^2} \Bigg/ \frac{\mathrm{d}\sigma^{e^+e^-\to e^+e^-\rho_{\mathrm{L}}\rho_{\mathrm{L}}}}{\mathrm{d}t\,\mathrm{d}y_1\,\mathrm{d}y_2\,\mathrm{d}Q_1^2\,\mathrm{d}Q_2^2} \simeq \frac{\alpha_{\mathrm{em}}^2 Q_1^4 Q_2^4}{\alpha_{\mathrm{s}}^4 s^2 m_\rho^4}\,, \tag{55}$$

which is suppressed at ILC energies, and it would be of comparable order of magnitude only for colliders with CMS energy of the order of a few GeV.

5.3 Results for cross-section

The cross-sections $\frac{\mathrm{d}\sigma^{e^+e^-\to e^+e^-\rho_{\mathrm{L}}\rho_{\mathrm{L}}}}{\mathrm{d}t}$ are displayed in Fig. 15. They are shown as functions of t for different polarizations and plotted after integrating the differential cross-section in (49) over the phase space considered previously. We made the following assumptions: we choose the QCD coupling constant to be $\alpha_{\mathrm{s}}(\sqrt{Q_1 Q_2})$ running at three loops, the parameter $c = 1$ which enters in the Regge limit condition and the cm energy $\sqrt{s} = 500\,\mathrm{GeV}$. Figure 15 shows for e^+e^- scattering the same differential cross-sections as Fig. 5, but related to different photon helicities. We see that the shapes of the corresponding curves are similar, although they lead to quite different values of the cross-sections. The cross-sections corresponding to photons with at least one transverse polarization vanish as

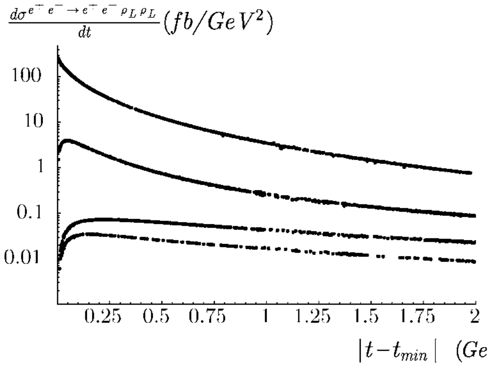

Fig. 15. Cross-sections for $e^+e^- \to e^+e^-\rho_L^0\rho_L^0$ process. Starting from above, we display the cross-sections corresponding to the $\gamma_L^*\gamma_L^*$ mode, to the $\gamma_L^*\gamma_T^*$ modes, to the $\gamma_T^*\gamma_{T'}^*$ modes with different $T \neq T'$ and finally to the $\gamma_T^*\gamma_{T'}^*$ modes with the same $T = T'$

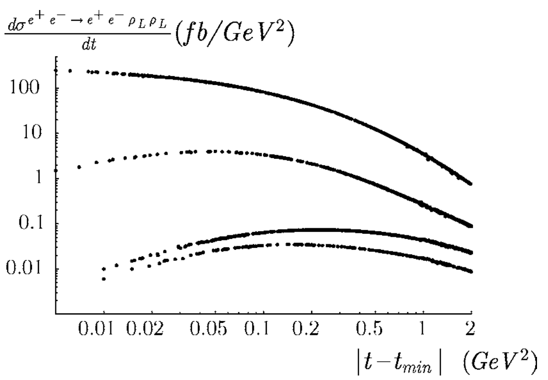

Fig. 16. Cross-sections for $e^+e^- \to e^+e^-\rho_L^0\rho_L^0$ process, in log-log scale. Starting from above, we display the cross-sections corresponding to the $\gamma_L^*\gamma_L^*$ mode, to the $\gamma_L^*\gamma_T^*$ modes, to the $\gamma_T^*\gamma_{T'}^*$ modes with different $T \neq T'$ and finally to the $\gamma_T^*\gamma_{T'}^*$ modes with the same $T = T'$

in the $\gamma^*\gamma^*$ case at $t = t_{\min}$ (cf. Sect. 4.2). Similarly, each of them has a maximum in the very small t region. These maxima are shown more accurately on the log–log plot in Fig. 16.

At this point one technical remark is in order. By looking into the upper plot in Fig. 16 related to the $\mathcal{M}_{00}$ amplitude, one sees that the points corresponding to non-zero $|t - t_{\min}|$ approach smoothly the point on the axis $|t - t_{\min}| = 0$. This point $|t - t_{\min}| = 0$ is of special interest, because it gives the maximum of the total cross-section (since the transverse polarization case vanishes at $t_{\min}$) and then practically dictates the trend of the total cross-section, which is strongly peaked in the forward direction (for the longitudinal case) and strongly decreases with t (for all polarizations), as shown already at the level of the $\gamma^*\gamma^*$ cross-sections in Sect. 4.2. Due to numerical instabilities, the differential cross-section at $|t - t_{\min}| = 0$ must be evaluated in a different way than those for $|t - t_{\min}| \neq 0$, i.e. by the use of (38), in which the integration over z_i was already done in the analytic way. Since (38) involves several polylogarithmic functions, its structure of cuts is quite inconvenient for further numerical integration over the variables y_i and Q_i. In order to overcome this technical problem it is useful to rewrite (38) by the use of the Euler identity [48] in the form

$$\begin{aligned}\mathcal{M}_{00} = &-\mathrm{i}s\frac{N_c^2-1}{N_c^2}\alpha_s^2\alpha_{\mathrm{em}}f_\rho^2\frac{9\pi^2}{2}\frac{1}{Q_1^2Q_2^2}\left[6\left(R+\frac{1}{R}\right)\ln^2 R\right.\\&+12\left(R-\frac{1}{R}\right)\ln R+12\left(R+\frac{1}{R}\right)\\&+\left(3R^2+2+\frac{3}{R^2}\right)\left(\left(\frac{\pi^2}{6}-\mathrm{Li}_2(1-R)\right)\ln R\right.\\&-\ln(R+1)\ln^2 R-2\mathrm{Li}_2(-R)\ln R+\mathrm{Li}_2(R)\ln R\\&\left.\left.+2\mathrm{Li}_3(-R)-2\mathrm{Li}_3(R)\right)\right], \qquad (56)\end{aligned}$$

since now the imaginary terms only come from $\mathrm{Li}_2(R)$ and $\mathrm{Li}_3(R)$ along their cuts, which cancel among each other analytically. Therefore, one can safely use their real part in a numerical fortran code as defined in standard packages.

The ILC collider is expected to run at a CMS nominal energy of 500 GeV, though it might be extended in order to cover a range between 200 GeV and 1 TeV. Because of this possibility, we below discuss how the change of the energy in CMS influences our predictions for the cross-sections measured in the same BeamCal detector. Furthermore, we discuss the effects of our various assumptions on the cross-section $\frac{\mathrm{d}\sigma^{e^+e^-\to e^+e^-\rho_L\rho_L}}{\mathrm{d}t}$ at the point $t_{\min}$, and consequently on the behavior of the total cross-section.

Figure 17 shows the cross-section at $t_{\min}$ as a function of the CMS energy $\sqrt{s}$ for different choices of the strong coupling constant α_s. To see the sensitivity of our predictions to these choices, we plot the cross-section at $t_{\min}$ in two cases: the blue curve corresponds to $\alpha_s(\sqrt{Q_1Q_2})$ running at one loop and the red one to $\alpha_s(\sqrt{Q_1Q_2})$ running at three loops. The curves in Fig. 17 are very close to each other, which leads to a small uncertainty on the total cross-section as we will see in the following.

The shapes of plots in Fig. 17 distinguish two different domains: if the planned CMS energy range $\sqrt{s}$ is lower than 500 GeV, the function $f(Q_i)$ (cf. (51)) appearing as a constraint on the minimum value of y_i in the phase space integration domain does not play any role at $\theta_{\min} = 4\,\mathrm{mrad}$. Thus the cross-section increases with $\sqrt{s}$ between 200 and 500 GeV. Because of the condition we assumed on the minimal value of the energies of the scattered leptons in Sect. 5.1, the y_i integration domain becomes very narrow (cf. (52)) when $\sqrt{s}$ goes to 200 GeV and leads to a strong decreasing of the cross-section at this CMS energy. Note that if $\sqrt{s}$ becomes bigger than 500 GeV, $f(Q_i)$ will cut the small y_i region (which contributes mainly because of the Weizsäcker–Williams photons fluxes) when $\sqrt{s}$ increases. Thus the cross-section falls down between 500 GeV and 1 TeV. This is due to the limitation caused by the minimal detection angle offered by the BeamCal calorimeter, which is thus optimal for our process when $\sqrt{s} = 500$ GeV. This effect on $f(Q_i)$ could be compensated if one could increase the value of Q_i, but this would be completely suppressed because of the strong decreasing of the amplitude with Q_i. The above discussion leads also to the conclusion

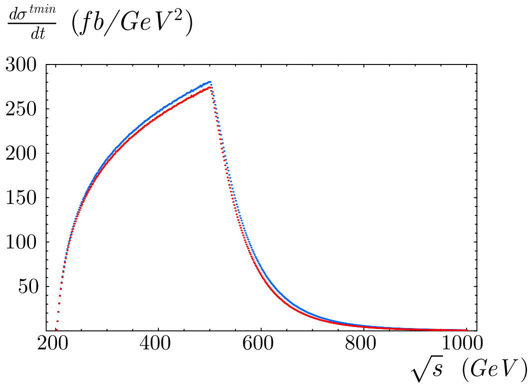

Fig. 17. Cross-sections for $e^+e^- \to e^+e^-\rho^0_{\mathrm{L}}\rho^0_{\mathrm{L}}$ at $t = t_{\mathrm{min}}$ for different α_{s}: the *blue* and *red curves* for α_{s} running respectively at one and three loops, with $c = 1$

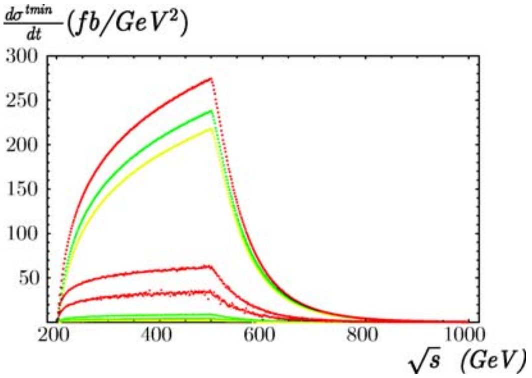

Fig. 18. Cross-sections for $e^+e^- \to e^+e^-\rho^0_{\mathrm{L}}\rho^0_{\mathrm{L}}$ at $t = t_{\mathrm{min}}$ for different values of the parameter c: the *red* [*black*] *curves* correspond to $c = 1$, the *green* [*dark grey*] *curves* to $c = 2$ and and the *yellow* [*light grey*] curves to $c = 3$. For each value of c, by decreasing order the curves correspond to gluon exchange, quark exchange with longitudinal virtual photons and quark exchange with transverse virtual photons

that, although the Born order cross-sections do not depend on s, the triggering effects introduce an s-dependence of the measured cross-sections.

Figure 18 shows the cross-section at t_{min} for different values of the parameter c, which enters in the Regge limit condition $s_{\gamma^*\gamma^*} = y_1y_2s > cQ_1Q_2$. The value of the parameter c controls the dominance of gluonic contributions to the scattering amplitude: the increase of c should lead to suppression of quark exchanges. To see that we display the quark contribution in the same bins, we use the usual phase space for the process $e^+e^- \to e^+e^-\rho^0_{\mathrm{L}}\rho^0_{\mathrm{L}}$ (cf. (5)) with the expressions of the amplitudes (43) and (44), and we perform their numerical integration on y_i and Q_i with the same cuts as in the two gluon exchange process (cf. Sect. 5.1). For each value of c we plot the three curves corresponding to the two gluon exchange process and the quark exchange processes with longitudinal and transverse virtual photons.

A technical remark is in order when performing this integration numerically. Equation (44) is not divergent when $Q_i^2 \to s$, because this limit is only valid if $s(1 - Q_1^2/s)\times(1 - Q_2^2/s)$ is finite and positive since this term corresponds in our notation to the CMS energy of the virtual photons. In order to avoid numerical instabilities we add the condition $y_1y_2s > Q_1^2, Q_2^2$ to the Regge limit condition. We can check that this supplementary constraint does not change our results for the other contributions, namely for processes with two gluon exchange and quark exchange with longitudinal virtual photons.

As expected, the quark contribution is suppressed when increasing c and becomes completely negligible as soon as c exceeds 2. The whole discussion above concerned the case $t = t_{\mathrm{min}}$, which determines the general trend of the cross-section in the non-forward case. Because of that, we hope that the above conclusions are also valid at the level of the cross-section integrated over t. Thus, we omit below the quark exchanges.

We finally obtain the following results for the total cross-section integrated over t. We shall show three different predictions, which differ by the choice of the definition of the coupling constant and by the choice of the value of the parameter c controlling the gluon dominance. First we choose $\alpha_{\mathrm{s}}(\sqrt{Q_1Q_2})$ running at three loops, the constant $c = 1$, the CMS energy $\sqrt{s} = 500$ GeV and we obtain (up to numerical uncertainties)

$$\begin{aligned}\sigma^{\mathrm{LL}} &= 32.4\,\mathrm{fb}\,,\\ \sigma^{\mathrm{LT}} &= 1.5\,\mathrm{fb}\,,\\ \sigma^{\mathrm{TT}} &= 0.2\,\mathrm{fb}\,,\end{aligned} \tag{57}$$

and then

$$\sigma^{\mathrm{Total}} = 34.1\,\mathrm{fb}\,. \tag{58}$$

With a nominal integrated luminosity of 125 fb^{-1}, this will yield 4.26×10^3 events per year.

Secondly, with the choice of $\alpha_{\mathrm{s}}(\sqrt{Q_1Q_2})$ running at one loop, the constant $c = 1$ and the CMS energy $\sqrt{s} =$ .500 GeV, we obtain

$$\begin{aligned}\sigma^{\mathrm{LL}} &= 33.9\,\mathrm{fb}\,,\\ \sigma^{\mathrm{LT}} &= 1.5\,\mathrm{fb}\,,\\ \sigma^{\mathrm{TT}} &= 0.2\,\mathrm{fb}\,,\end{aligned} \tag{59}$$

which leads to

$$\sigma^{\mathrm{Total}} = 35.6\,\mathrm{fb}\,. \tag{60}$$

As expected, we see that the transition from three to one loop changes the total cross-section very little. This result will yield 4.45×10^3 events per year with a nominal integrated luminosity of 125 fb^{-1}.

In the third choice, we choose $\alpha_{\mathrm{s}}(\sqrt{Q_1Q_2})$ running at three loops, the same CMS energy $\sqrt{s} = 500$ GeV and the constant $c = 2$ (for which as previously discussed quark exchanges are completely negligible) and we get

$$\begin{aligned}\sigma^{\mathrm{LL}} &= 28.1\,\mathrm{fb}\,,\\ \sigma^{\mathrm{LT}} &= 1.3\,\mathrm{fb}\,,\\ \sigma^{\mathrm{TT}} &= 0.2\,\mathrm{fb}\,,\end{aligned} \tag{61}$$

which imply

$$\sigma^{\mathrm{Total}} = 29.6\,\mathrm{fb}\,. \tag{62}$$

This result will yield 3.7×10^3 events per year with a nominal integrated luminosity of $125\,\mathrm{fb}^{-1}$.

Finally, we also consider the same assumptions as the previous ones except for the value of the constant c, which is now set to $c = 10$ in order to consider a more drastic Regge limit condition, and we obtain

$$\begin{aligned} \sigma^{\mathrm{LL}} &= 19.3\,\mathrm{fb}\,,\\ \sigma^{\mathrm{LT}} &= 0.9\,\mathrm{fb}\,,\\ \sigma^{\mathrm{TT}} &= 0.11\,\mathrm{fb}\,, \end{aligned} \tag{63}$$

which leads to

$$\sigma^{\mathrm{Total}} = 20.3\,\mathrm{fb}\,. \tag{64}$$

This result will yield 2.5×10^3 events per year with a nominal integrated luminosity of $125\,\mathrm{fb}^{-1}$. Thus, this shows that the precise way one implements the restriction of the kinematical phase space to the domain of applicability of the impact representation does not dramatically change the number of events.

The whole prediction above was obtained using the asymptotical DA. In order to see the sensitivity of this assumption on our results, we also do the calculation using the DA (37) within different models. The choice of the DA of [49] with $a_2 = -0.1$ and $a_4 = 0$ gives 4.2×10^3 events per year, while the choice of the DA of [50] with $a_2 = 0.05$ and $a_4 = 0$ gives 4.3×10^3 events per year.

In summary of this part we see that our predictions are quite stable when changing the main parameters characterizing the theoretical uncertainties of our approach.

The obvious question that appears now is how our predictions summarized by (58)–(62) will change by the inclusion of the BFKL resummation effects. Generally BFKL evolution strongly increases the values of the cross-sections, which means that usually the results obtained in Born approximation can be considered as a lower limit of the cross-sections for ρ-meson pair production with complete BFKL evolution taken into account. Although the complete analysis of the BFKL evolution for our process is beyond the scope of the present paper, we would like to finish this section with a few remarks on the possible effects caused by the BFKL evolution.

We consider below only the point $t = t_{\mathrm{min}}$ and we restrict ourselves to the leading order BFKL evolution.[4] Of course, such an estimate should be taken with great caution, since it is well known that LO BFKL overestimates the magnitude of corrections.

In Fig. 19 we show the corresponding cross-section at t_{min} as a function of $\sqrt{s}$, for different choices of α_{s}: we considered α_{s} running at one and three loops (red curves) as in the previous discussion for the two gluon exchange, and we also used a fixed value of α_{s} (green curve) corresponding to the three loop running coupling constant at a typical virtuality of $Q = 1.1$ GeV. We have used the expression of the BFKL amplitude [23, 24] for the forward case in the saddle point approximation, namely

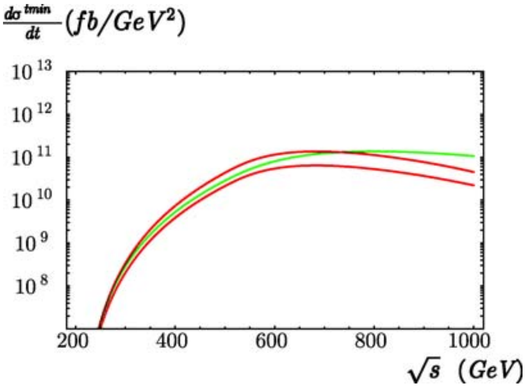

Fig. 19. Cross-sections for $e^+e^- \to e^+e^-\rho_{\mathrm{L}}^0\rho_{\mathrm{L}}^0$ with LO BFKL evolution at $t = t_{\mathrm{min}}$ for different α_{s} : the *upper* and *lower red curves* for α_{s} running respectively at one and three loops and the *green one* (the *middle curve*) for $\alpha_{\mathrm{s}} = 0.46$

$$\begin{aligned} &A(s, t = t_{\mathrm{min}}, Q_1, Q_2)\\ &\quad\sim \mathrm{i}s\pi^5\sqrt{\pi}\frac{9\left(N_c^2-1\right)}{4N_c^2}\frac{\alpha_{\mathrm{s}}^2\alpha_{\mathrm{em}}f_\rho^2}{Q_1^2Q_2^2}\frac{\mathrm{e}^{4\ln 2\bar{\alpha}_{\mathrm{s}}Y}}{\sqrt{14\bar{\alpha}_{\mathrm{s}}\zeta(3)Y}}\\ &\quad\times\exp\left(-\frac{\ln^2 R}{14\bar{\alpha}_{\mathrm{s}}\zeta(3)Y}\right), \end{aligned} \tag{65}$$

with the rapidity $Y = \ln\left(\frac{c' s y_1 y_2}{Q_1 Q_2}\right)$, $\bar{\alpha}_{\mathrm{s}} = \frac{N_c}{\pi}\alpha_{\mathrm{s}}(\sqrt{Q_1 Q_2})$ and $R = \frac{Q_1}{Q_2}$. The plots in Fig. 19 are obtained by assuming that the constant c' in (65), which at LO is arbitrary and of order 1, is chosen to be 1. The factor $\exp(4\ln 2\bar{\alpha}_{\mathrm{s}}Y)$ explains the enhancement of the sensitivity to the choice of α_{s} compared to the one in the Born two gluon exchange case, since $4\ln 2Y$ takes big values for the ILC rapidities Y. For the same reasons as discussed earlier in this section, the function $f(Q_i)$ does not appear for $\sqrt{s}$ lower than 500 GeV; the LO BFKL cross-section then grows exponentially with s in this domain. The effect of $f(Q)$ starting from 500 GeV gives an inflection point of the curves and a maximum beyond 500 GeV; then the curves decrease until 1 TeV.

The effect of varying the parameter c' in the BFKL prediction is illustrated in Fig. 20. As expected, it has a strong effect on the order of magnitude of the differential cross-section, since the rapidity is very high and thus leads to a large value of the factor $\exp(4\ln 2\bar{\alpha}_{\mathrm{s}}Y)$, which is highly sensitive to the precise definition of the rapidity.

Comparing the order of magnitude of the Born cross-section (Figs. 17 and 18) with cross-sections provided by the LO BFKL evolution (Figs. 19 and 20), one could be astonished by the fact that they differ by several orders of magnitudes. From previous studies at the level of $\gamma^*\gamma^*$ [23, 24, 38], the NLO contribution is known to be between the LO and the Born order cross-section. Thus, at the level of the e^+e^- process, such a large magnitude for

---

[4] Note that related studies with a hard scale provided by t and not by Q^2 were performed in [51, 52].

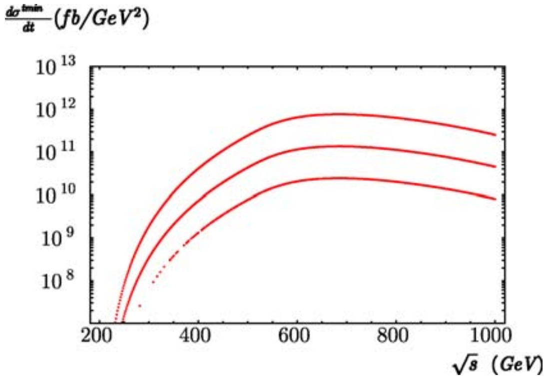

Fig. 20. LO BFKL cross-section for $e^+e^- \to e^+e^-\rho^0_{\rm L}\rho^0_{\rm L}$ at $t = t_{\min}$ for different values of the parameter c': by decreasing order, the curves correspond to $c' = 2$, $c' = 1$ and $c' = 0.5$. c is fixed to be equal to 1

the LO BFKL cross-section will be suppressed at NLO, leading to a more realistic estimate.

The above discussion of BFKL enhancement was restricted to the forward case, $t = t_{\min}$. In the non-forward case, the phase-space region with small t values dominates the cross-sections. The obtained hierarchy between cross-sections in Born approximation for different photon polarizations will presumably still be valid when including BFKL evolution at any order of resummation (LO, NLO, etc.). Indeed, the argument given in Sect. 4.2 for the Born order, and on which this hierarchy is based, only relies on the s-channel helicity conservation. Technically, it is based on the impact representation, which is valid beyond Born and/or LO approximation.

The comparison of Figs. 17 and 18 with Figs. 19 and 20 leads to the conclusions that the BFKL evolution changes the shape of the cross-section: when increasing $\sqrt{s}$ from 500 GeV to 1 TeV, the two gluon exchange cross-section will fall down, while with the BFKL resummation effects, the cross-section should more or less be stable, with a high number of events still to be observed for these CMS energies.

6 Conclusion

The present study should be considered as a continuation of our previous investigations [19–24] for the production of two $\rho^0_{\rm L}$ mesons in the scattering of two longitudinally polarized virtual photons. The diffractive production of a meson pair is one of the gold plated processes that permit clean studies of the BFKL dynamics at ILC. Our main motivation in the present work was to estimate, in the Born approximation, the cross-section for the production of $\rho^0_{\rm L}$-meson pairs in the e^+e^- collisions occurring in the kinematical conditions of the future ILC. For this aim, we first calculated contributions, missing up to now, that involve the helicity amplitudes with transversally polarized virtual photons. This was done in a mostly analytic way, by the use of techniques developed in [22]. Having done so, we calculated the cross-section for the electroproduction of $\rho^0_{\rm L}$-meson pairs that takes into account the kinematical cuts imposed by the LDC design project for the BeamCal detector. By assuming a nominal value for the integrated luminosity, we predict (in the numerical analysis of cross-sections) a production of at least 4×10^3 meson pairs per year, a value which is sufficiently large to ensure a reliable data analysis.

We discussed a possible background process in the BeamCal detector that can identify in a misleading way an outgoing lepton with a photon. We predict that the cross-section for such a background process is negligibly small at ILC energies.

Finally, we discussed theoretical uncertainties of the estimates obtained. There are two main sources of them. The first one is related to the assumptions we have made to characterize the Regge limit and the particular role played by the parameter c; we also observe a sensitivity of our results on the choice of the running coupling constant.

The second source of theoretical uncertainties of our estimates is related to taking into account the effects of the BFKL evolution. Generally, inclusion of the BFKL evolution significantly increases the cross-section, as one sees from comparison of Fig. 17 with Fig. 19, obtained within the LO BFKL approach. On the other hand, it is known that this increase of predictions for the cross-sections is smaller if the BFKL evolution is considered at the next-to-leading order. Because of this we can safely say that our predictions should be considered as a lower limit for the predictions that are obtained by taking into account BFKL effects at NLO. We hope to consider this issue in our future publications.

In principle, the same techniques can be applied for the description of processes involving other final states, both with positive charge parity exchange in t-channel, e.g. J/Ψ pairs, as well as negative charge parity, e.g. $\gamma^*\gamma^* \to \eta_c\eta_c$ [53].

Acknowledgements. We thank G. Korchemsky, S. Munier, B. Pire, R. Poeschl and F. Richard for many discussions and comments. This work is supported by the Polish Grant 1 P03B 028 28, the French–Polish scientific agreement Polonium. L.S. is a visiting fellow of the Fonds National pour la Recherche Scientifique (Belgium).

Appendix

In this appendix we collect the analytical expressions of the coefficients $a(\underline{r}; Q_1, Q_2; z_1, z_2)$, $b(\underline{r}; Q_1, Q_2; z_1, z_2)$ and $f(\underline{r}; Q_1, Q_2; z_1, z_2)$, as well as all the generic integrals that appear in the computation of the Born amplitude in Sect. 4. The coefficients a, b and f can be expressed as combinations of several generic integrals:

$$
\begin{aligned}
&a(\underline{r}; Q_1, Q_2; z_1, z_2)\\
&= \frac{1}{2}[I_{3\mu_1\mu_2}(z_1, z_2) + I_{3\mu_1\mu_2}(\bar{z}_1, \bar{z}_2)\\
&\quad - I_{3\mu_1\mu_2}(\bar{z}_1, z_2) - I_{3\mu_1\mu_2}(z_1, \bar{z}_2)]
\end{aligned}
$$

$$
\begin{aligned}
&-\frac{r^2}{2}\left[I_{4\mu_1\mu_2}(z_1,z_2)-I_{4\mu_1\mu_2}(\bar z_1,z_2)\right]\\
&-\frac{1}{r^2}\Big[J^c_{\mu_1\mu_2}(z_1,\bar z_2)+J^c_{\mu_1\mu_2}(\bar z_1,z_2)\\
&\qquad -J^c_{\mu_1\mu_2}(\bar z_1,\bar z_2)-J^c_{\mu_1\mu_2}(z_1,z_2)\Big]\,, \qquad \text{(A.1)}
\end{aligned}
$$

$$
\begin{aligned}
&b(\underline{r};Q_1,Q_2;z_1,z_2)\\
&=\Bigg[\frac{z_1z_2}{\left(z_1^2\underline{r}^2+\mu_1^2\right)\left(z_2^2\underline{r}^2+\mu_2^2\right)}-\frac{z_1\bar z_2}{\left(z_1^2\underline{r}^2+\mu_1^2\right)\left(\bar z_2^2\underline{r}^2+\mu_2^2\right)}\\
&\quad-\frac{\bar z_1z_2}{\left(\bar z_1^2\underline{r}^2+\mu_1^2\right)\left(z_2^2\underline{r}^2+\mu_2^2\right)}+\frac{\bar z_1\bar z_2}{\left(\bar z_1^2\underline{r}^2+\mu_1^2\right)\left(\bar z_2^2\underline{r}^2+\mu_2^2\right)}\Bigg]r^2I_2\\
&\quad+\Bigg(\left[\frac{z_1}{z_1^2\underline{r}^2+\mu_1^2}-\frac{\bar z_1}{\bar z_1^2\underline{r}^2+\mu_1^2}\right]\\
&\quad\times\left[I_{2\mu_2}(\bar z_2)-I_{2\mu_2}(z_2)+r^2(\bar z_2-z_2)I_{3\mu_2}(z_2)\right]+(1\leftrightarrow 2)\Bigg)\\
&\quad+r^2\left[\frac{1}{2}+2z_1z_2-(z_1+z_2)\right]\\
&\quad\times\left[I_{4\mu_1\mu_2}(z_1,z_2)+I_{4\mu_1\mu_2}(z_1,\bar z_2)\right]\\
&\quad+\left[-\frac{1}{2}+(z_1+z_2)\right]I_{3\mu_1\mu_2}(z_1,z_2)\\
&\quad+\left[\frac{3}{2}-(z_1+z_2)\right]I_{3\mu_1\mu_2}(\bar z_1,\bar z_2)\\
&\quad+\left[z_1-z_2-\frac{1}{2}\right]I_{3\mu_1\mu_2}(\bar z_1,z_2)\\
&\quad+\left[z_2-z_1-\frac{1}{2}\right]I_{3\mu_1\mu_2}(z_1,\bar z_2)]\\
&\quad+\frac{1}{r^2}\Big[J^c_{\mu_1\mu_2}(z_1,\bar z_2)+J^c_{\mu_1\mu_2}(\bar z_1,z_2)\\
&\quad-J^c_{\mu_1\mu_2}(\bar z_1,\bar z_2)-J^c_{\mu_1\mu_2}(z_1,z_2)\Big]\,, \qquad \text{(A.2)}
\end{aligned}
$$

$$
\begin{aligned}
&f(\underline{r};Q_1,Q_2;z_1,z_2)\\
&=\left[\frac{1}{z_1^2\underline{r}^2+\mu_1^2}+\frac{1}{\bar z_1^2\underline{r}^2+\mu_1^2}\right]\left[\frac{z_2}{z_2^2\underline{r}^2+\mu_2^2}-\frac{\bar z_2}{\bar z_2^2\underline{r}^2+\mu_2^2}\right]I_2\\
&\quad+2\left[\frac{\bar z_2}{\bar z_2^2\underline{r}^2+\mu_2^2}-\frac{z_2}{z_2^2\underline{r}^2+\mu_2^2}\right]I_{3\mu_1}(z_1)\\
&\quad+(\bar z_2-z_2)\left[\frac{1}{z_1^2\underline{r}^2+\mu_1^2}+\frac{1}{\bar z_1^2\underline{r}^2+\mu_2^2}\right]I_{3\mu_2}(z_2)\\
&\quad+(z_2-\bar z_2)\left[I_{4\mu_1\mu_2}(z_1,z_2)+I_{4\mu_1\mu_2}(\bar z_1,z_2)\right]\\
&\quad+\frac{1}{r^2}\left[\frac{1}{z_1^2\underline{r}^2+\mu_1^2}+\frac{1}{\bar z_1^2\underline{r}^2+\mu_1^2}\right]\left[I_{2\mu_2}(\bar z_2)-I_{2\mu_2}(z_2)\right]\\
&\quad+\frac{1}{r^2}\big[I_{3\mu_1\mu_2}(\bar z_1,z_2)-I_{3\mu_1\mu_2}(z_1,\bar z_2)\\
&\quad+I_{3\mu_1\mu_2}(z_1,z_2)-I_{3\mu_1\mu_2}(\bar z_1,\bar z_2)\big]\,, \qquad \text{(A.3)}
\end{aligned}
$$

part of which are divergent integrals:

$$I_2=\int\frac{\mathrm{d}^d\underline{k}}{\underline{k}^2(\underline{k}-\underline{r})^2}\,, \qquad \text{(A.4)}$$

$$I_{2m}(a)=\int\frac{\mathrm{d}^d\underline{k}}{\underline{k}^2\left((\underline{k}-a\underline{r})^2+m^2\right)}\,, \qquad \text{(A.5)}$$

$$I_{3m}(a)=\int\frac{\mathrm{d}^d\underline{k}}{\underline{k}^2(\underline{k}-\underline{r})^2\left((\underline{k}-a\underline{r})^2+m^2\right)}\,, \qquad \text{(A.6)}$$

$$I_{3m_am_b}(a,b)=\int\frac{\mathrm{d}^d\underline{k}}{\underline{k}^2\left((\underline{k}-a\underline{r})^2+m_a^2\right)\left((\underline{k}-b\underline{r})^2+m_b^2\right)}\,, \qquad \text{(A.7)}$$

$$
\begin{aligned}
&I_{4m_am_b}(a,b)\\
&\quad=\int\frac{\mathrm{d}^d\underline{k}}{\underline{k}^2(\underline{k}-\underline{r})^2\left((\underline{k}-a\underline{r})^2+m_a^2\right)\left((\underline{k}-b\underline{r})^2+m_b^2\right)}\,, \qquad \text{(A.8)}
\end{aligned}
$$

and some of them are finite:

$$J_{2m_am_b}(a,b)=\int\frac{\mathrm{d}^d\underline{k}}{\left((\underline{k}-a\underline{r})^2+m_a^2\right)\left((\underline{k}-b\underline{r})^2+m_b^2\right)}\,, \qquad \text{(A.9)}$$

$$J^c_{m_am_b}(a,b)=\int\frac{\mathrm{d}^d\underline{k}(\underline{k}\cdot\underline{r})}{\underline{k}^2\left((\underline{k}-a\underline{r})^2+m_a^2\right)\left((\underline{k}-b\underline{r})^2+m_b^2\right)}\,, \qquad \text{(A.10)}$$

$$
\begin{aligned}
K_{m_am_b}(a,b)=\int\frac{\mathrm{d}^d\underline{k}}{\underline{k}^2}\Bigg[&\frac{1}{\left(b^2\underline{r}^2+m_b^2\right)\left[(\underline{k}-a\underline{r})^2+m_a^2\right]}\\
&+\frac{1}{\left(a^2\underline{r}^2+m_a^2\right)\left[(\underline{k}-b\underline{r})^2+m_b^2\right]}\\
&-\frac{2r^2}{\left[\underline{k}^2+(\underline{r}-\underline{k})^2\right]\left(a^2\underline{r}^2+m_a^2\right)\left(b^2\underline{r}^2+m_b^2\right)}\Bigg], \qquad \text{(A.11)}
\end{aligned}
$$

$$
\begin{aligned}
L_{m_am_b}(a,b)=\int\frac{\mathrm{d}^d\underline{k}}{\underline{k}^2}\Bigg[&\frac{1}{\left(a^2\underline{r}^2+m_a^2\right)\left[(\underline{k}-b\underline{r})^2+m_b^2\right]}\\
&-\frac{r^2}{\left[\underline{k}^2+(\underline{r}-\underline{k})^2\right]\left(a^2\underline{r}^2+m_a^2\right)\left(b^2\underline{r}^2+m_b^2\right)}\Bigg], \qquad \text{(A.12)}
\end{aligned}
$$

$$
\begin{aligned}
N_{m_am_b}(a,b)=\int\frac{\mathrm{d}^d\underline{k}}{\underline{k}^2}\Bigg[&\frac{1}{\left(a^2\underline{r}^2+m_a^2\right)\left[(\underline{k}-b\underline{r})^2+m_b^2\right]}\\
&-\frac{1}{\left(b^2\underline{r}^2+m_b^2\right)\left[(\underline{k}-a\underline{r})^2+m_a^2\right]}\Bigg], \qquad \text{(A.13)}
\end{aligned}
$$

$$
\begin{aligned}
J_{3\mu}(a)=\int\frac{\mathrm{d}^2\underline{k}}{\underline{k}^2(\underline{k}-\underline{r})^2}\Bigg[&\frac{1}{(\underline{k}-\underline{r}a)^2+\mu^2}-\frac{1}{a^2\underline{r}^2+\mu^2}\\
&+(a\leftrightarrow\bar a)\Bigg]\,, \qquad \text{(A.14)}
\end{aligned}
$$

$$
\begin{aligned}
J_{4\mu_1\mu_2}(z_1,z_2)=\int&\frac{\mathrm{d}^2\underline{k}}{\underline{k}^2(\underline{k}-\underline{r})^2}\\
&\times\Bigg[\frac{1}{\left((\underline{k}-\underline{r}z_1)^2+\mu_1^2\right)\left((\underline{k}-\underline{r}z_2)^2+\mu_2^2\right)}\\
&-\frac{1}{\left(z_1^2\underline{r}^2+\mu_1^2\right)\left(z_2^2\underline{r}^2+\mu_2^2\right)}+(z\leftrightarrow\bar z)\Bigg]. \qquad \text{(A.15)}
\end{aligned}
$$

Although the divergent integrals (A.4)–(A.8) enter (A.1)–(A.3), the coefficients $a(\underline{r};Q_1,Q_2;z_1,z_2)$, $b(\underline{r};Q_1,Q_2;z_1,z_2)$ and $f(\underline{r};Q_1,Q_2;z_1,z_2)$ are finite expressions. To see this requires tracing of the cancellation of divergencies within each of these coefficients, which in principle can be done within a dimensional regularization scheme. Unfortunately, this procedure is not always practically feasible, especially for the integrals I_{3m}, $I_{3m_1m_2}$ or

$I_{4m_1m_2}$, which apart of massless propagators contain also massive propagators. These integrals can be rewritten in terms of the simpler, although divergent integrals I_2 and I_{2m} as

$$\begin{aligned}
&I_{3m_1m_2}(z_1,z_2)\\
&=-\frac{1}{2}\left(\frac{1}{z_1^2\underline{r}^2+m_1^2}+\frac{1}{z_2^2\underline{r}^2+m_2^2}\right)J_{2m_1m_2}(z_1,z_2)\\
&\quad+\left(\frac{z_1}{z_1^2\underline{r}^2+m_1^2}+\frac{z_2}{z_2^2\underline{r}^2+m_2^2}\right)J^c_{m_1m_2}(z_1,z_2)\\
&\quad+\frac{1}{2\left(z_2^2\underline{r}^2+m_2^2\right)}I_{2m_1}(z_1)+\frac{1}{2\left(z_1^2\underline{r}^2+m_1^2\right)}I_{2m_2}(z_2)\,,
\end{aligned}\tag{A.16}$$

$$\begin{aligned}
&I_{4m_1m_2}(z_1,z_2)\\
&=\frac{1}{2}\left(\frac{1}{\left(z_1^2\underline{r}^2+m_1^2\right)\left(z_2^2\underline{r}^2+m_2^2\right)}\right.\\
&\quad\left.+\frac{1}{\left(\bar{z}_1^2\underline{r}^2+m_1^2\right)\left(\bar{z}_2^2\underline{r}^2+m_2^2\right)}\right)I_2+\frac{1}{2}J_{4m_1m_2}(z_1,z_2)\,,
\end{aligned}\tag{A.17}$$

$$\begin{aligned}
&I_{3m}(z)\\
&=\frac{1}{2}\left(\frac{1}{z^2\underline{r}^2+m^2}+\frac{1}{\bar{z}^2\underline{r}^2+m^2}\right)I_2+\frac{1}{2}J_{3m}(z)\,.
\end{aligned}\tag{A.18}$$

Divergent integrals like I_2 and I_{2m} or finite ones like $J^c_{m_1m_2}$ and $J_{2m_1m_2}$ are directly computed by standard Feynman techniques.

The finite integrals $J_{4m_1m_2}$ and J_{3m} are calculated by the use of the change of variables defined by the inverse conformal transformation applied to the momenta and other dimensional parameters of integrals [18]. Such a change of variables applied to the two dimensional, UV and IR finite integrals results in a reduction of the number of massless propagators, a well known property from the studies of conformal field theories in coordinate space [54].

As a result, we get the following expressions for the coefficients $a(\underline{r};Q_1,Q_2;z_1,z_2)$, $b(\underline{r};Q_1,Q_2;z_1,z_2)$ and $f(\underline{r};Q_1,Q_2;z_1,z_2)$, which involve only explicitly convergent integrals:

$$\begin{aligned}
&a(\underline{r},z_1,z_2)\\
&=\left(\frac{1}{2}\left[\frac{z_1}{\left(z_1^2\underline{r}^2+\mu_1^2\right)}+\frac{z_2}{\left(z_2^2\underline{r}^2+\mu_2^2\right)}+\frac{1}{r^2}\right]J^c_{\mu_1\mu_2}(z_1,z_2)\right.\\
&\quad+\frac{1}{4}K(z_1,z_2)+(z_1\leftrightarrow\bar{z}_1,z_2\leftrightarrow\bar{z}_2)\\
&\quad\left.-(z_1\leftrightarrow\bar{z}_1)-(z_2\leftrightarrow\bar{z}_2)\right)\\
&\quad+\frac{r^2}{4}\left[J_{4\mu_1\mu_2}(\bar{z}_1,z_2)-J_{4\mu_1\mu_2}(z_1,z_2)\right]\\
&\quad+\frac{1}{4}\left[\frac{1}{\left(z_1^2\underline{r}^2+\mu_1^2\right)}+\frac{1}{\left(z_2^2\underline{r}^2+\mu_2^2\right)}\right.\\
&\quad\left.+\frac{1}{\left(\bar{z}_1^2\underline{r}^2+\mu_1^2\right)}+\frac{1}{\left(\bar{z}_2^2\underline{r}^2+\mu_2^2\right)}\right]\\
&\quad\times\left[J_{2\mu_1\mu_2}(\bar{z}_1,z_2)-J_{2\mu_1\mu_2}(z_1,z_2)\right]\,,
\end{aligned}\tag{A.19}$$

$$\begin{aligned}
&b(\underline{r},z_1,z_2)\\
&=\frac{r^2}{2}\left[\frac{z_1}{z_1^2\underline{r}^2+\mu_1^2}-\frac{\bar{z}_1}{\bar{z}_1^2\underline{r}^2+\mu_1^2}\right][\bar{z}_2-z_2]J_{3\mu_2}(z_2)+(1\leftrightarrow 2)\\
&\quad+r^2\left[\frac{1}{2}+2z_1z_2-(z_1+z_2)\right]\\
&\quad\times\left[J_{4\mu_1\mu_2}(z_1,z_2)+J_{4\mu_1\mu_2}(z_1,\bar{z}_2)\right]\\
&\quad+\left[-\frac{1}{2}+z_1+z_2\right]\left[\left(\frac{z_1}{z_1^2\underline{r}^2+\mu_1^2}+\frac{z_2}{z_2^2\underline{r}^2+\mu_2^2}\right)J^c_{\mu_1\mu_2}(z_1,z_2)\right.\\
&\quad\left.-\frac{1}{2}\left(\frac{1}{z_1^2\underline{r}^2+\mu_1^2}+\frac{1}{z_2^2\underline{r}^2+\mu_2^2}\right)J_{2\mu_1\mu_2}(z_1,z_2)\right]\\
&\quad+\left[\frac{3}{2}-(z_1+z_2)\right]\left[\left(\frac{\bar{z}_1}{\bar{z}_1^2\underline{r}^2+\mu_1^2}+\frac{\bar{z}_2}{\bar{z}_2^2\underline{r}^2+\mu_2^2}\right)J^c_{\mu_1\mu_2}(\bar{z}_1,\bar{z}_2)\right.\\
&\quad\left.-\frac{1}{2}\left(\frac{1}{\bar{z}_1^2\underline{r}^2+\mu_1^2}+\frac{1}{\bar{z}_2^2\underline{r}^2+\mu_2^2}\right)J_{2\mu_1\mu_2}(\bar{z}_1,\bar{z}_2)\right]\\
&\quad+\left[z_1-z_2-\frac{1}{2}\right]\left[\left(\frac{\bar{z}_1}{\bar{z}_1^2\underline{r}^2+\mu_1^2}+\frac{z_2}{z_2^2\underline{r}^2+\mu_2^2}\right)J^c_{\mu_1\mu_2}(\bar{z}_1,z_2)\right.\\
&\quad\left.-\frac{1}{2}\left(\frac{1}{\bar{z}_1^2\underline{r}^2+\mu_1^2}+\frac{1}{z_2^2\underline{r}^2+\mu_2^2}\right)J_{2\mu_1\mu_2}(\bar{z}_1,z_2)\right]\\
&\quad+\left[z_2-z_1-\frac{1}{2}\right]\left[\left(\frac{z_1}{z_1^2\underline{r}^2+\mu_1^2}+\frac{\bar{z}_2}{\bar{z}_2^2\underline{r}^2+\mu_2^2}\right)J^c_{\mu_1\mu_2}(z_1,\bar{z}_2)\right.\\
&\quad\left.-\frac{1}{2}\left(\frac{1}{z_1^2\underline{r}^2+\mu_1^2}+\frac{1}{\bar{z}_2^2\underline{r}^2+\mu_2^2}\right)J_{2\mu_1\mu_2}(z_1,\bar{z}_2)\right]\\
&\quad+\frac{1}{r^2}\left[J^c_{\mu_1\mu_2}(z_1,\bar{z}_2)+J^c_{\mu_1\mu_2}(\bar{z}_1,z_2)\right.\\
&\quad\left.-J^c_{\mu_1\mu_2}(\bar{z}_1,\bar{z}_2)-J^c_{\mu_1\mu_2}(z_1,z_2)\right]\\
&\quad+L_{\mu_1\mu_2}(\bar{z}_1,z_2)+L_{\mu_1\mu_2}(\bar{z}_2,z_1)\\
&\quad-\frac{1}{4}\left[K_{\mu_1\mu_2}(z_1,z_2)+K(\bar{z}_1,\bar{z}_2)\right.\\
&\quad\left.+K_{\mu_1\mu_2}(z_1,\bar{z}_2)+K_{\mu_1\mu_2}(\bar{z}_1,z_2)\right]\\
&\quad+\frac{z_2-z_1}{2}\left[N_{\mu_1\mu_2}(z_1,z_2)+N_{\mu_1\mu_2}(\bar{z}_2,\bar{z}_1)\right]\\
&\quad+\frac{z_1+z_2}{2}\left[N_{\mu_1\mu_2}(z_1,\bar{z}_2)+N_{\mu_1\mu_2}(z_2,\bar{z}_1)\right]\,,
\end{aligned}\tag{A.20}$$

$$\begin{aligned}
&f(\underline{r},z_1,z_2)\\
&=\left[\frac{\bar{z}_2}{\bar{z}_2^2\underline{r}^2+\mu_2^2}-\frac{z_2}{z_2^2\underline{r}^2+\mu_2^2}\right]J_{3\mu_1}(z_1)\\
&\quad+\frac{z_2-\bar{z}_2}{2}\left[J_{4\mu_1\mu_2}(z_1,z_2)+J_{4\mu_1\mu_2}(\bar{z}_1,z_2)\right.\\
&\quad\left.-\left(\frac{1}{z_1^2\underline{r}^2+\mu_1^2}+\frac{1}{\bar{z}_1^2\underline{r}^2+\mu_1^2}\right)J_{3\mu_2}(z_2)\right]\\
&\quad+\left(\frac{1}{r^2}\left[-\frac{1}{2}\left(\frac{1}{z_1^2\underline{r}^2+\mu_1^2}+\frac{1}{z_2^2\underline{r}^2+\mu_2^2}\right)J_{2\mu_1\mu_2}(z_1,z_2)\right.\right.\\
&\quad\left.+\left(\frac{z_1}{z_1^2\underline{r}^2+\mu_1^2}+\frac{z_2}{z_2^2\underline{r}^2+\mu_2^2}\right)J^c_{\mu_1\mu_2}(z_1,z_2)\right]\\
&\quad\left.-(z_1\leftrightarrow\bar{z}_1,z_2\leftrightarrow\bar{z}_2)+(z_1\leftrightarrow\bar{z}_1)-(z_2\leftrightarrow\bar{z}_2)\right)\\
&\quad+\frac{1}{2r^2}\left[N(\bar{z}_1,\bar{z}_2)-N(z_1,z_2)+N(z_1,\bar{z}_2)-N(\bar{z}_1,z_2)\right]\,.
\end{aligned}\tag{A.21}$$

The separation of divergent and finite parts in all integrals involved was done within the dimensional regularization with $d = 2 + 2\epsilon$. Thus, for the simplest integral I_{2m} the result reads

$$I_{2m}(a) = \frac{\pi}{\epsilon\left(a^2\underline{r}^2 + m^2\right)}\left(1 + \epsilon\left(\ln\pi - \Psi(1) - \ln m^2 + 2\ln\left(a^2\underline{r}^2 + m^2\right)\right)\right), \quad \text{(A.22)}$$

or, for its massless case,

$$I_2 = \frac{2\pi}{\underline{r}^2\epsilon}\left(1 + \epsilon\left(\ln\left(\pi\underline{r}^2\right) - \Psi(1)\right)\right). \quad \text{(A.23)}$$

We will use the finite part of I_2 and I_{2m} to compute the integrals in which they are involved. For example, we can write the finite integrals $K_{m_a m_b}$, $L_{m_a m_b}$ and $M_{m_a m_b}$ in terms of the finite part of these integrals, since the divergent parts ultimately cancel when we express them like

$$K_{m_1 m_2}(z_1, z_2) = \frac{1}{z_2^2\underline{r}^2 + m_2^2} I_{2m_1}(z_1) + \frac{1}{z_1^2\underline{r}^2 + m_1^2} I_{2m_2}(z_2) - \frac{r^2}{\left(z_1^2\underline{r}^2 + m_1^2\right)\left(z_2^2\underline{r}^2 + m_2^2\right)} I_2\,, \quad \text{(A.24)}$$

$$L_{m_1 m_2}(z_1, z_2) = \frac{1}{z_1^2\underline{r}^2 + m_1^2} I_{2m_2}(z_2) - \frac{r^2}{2\left(z_1^2\underline{r}^2 + m_1^2\right)\left(z_2^2\underline{r}^2 + m_2^2\right)} I_2\,, \quad \text{(A.25)}$$

$$N_{m_1 m_2}(z_1, z_2) = \frac{1}{z_1^2\underline{r}^2 + m_1^2} I_{2m_2}(z_2) - \frac{1}{z_2^2\underline{r}^2 + m_2^2} I_{2m_1}(z_1). \quad \text{(A.26)}$$

The integrals that involve only two massive propagators are finite and are calculated in a standard way using Feynman parameters. We obtain

$$J_{2m_a m_b} = \int \frac{\mathrm{d}^d\underline{k}}{\left((\underline{k} - \underline{r}a)^2 + m_a^2\right)\left((\underline{k} - \underline{r}b)^2 + m_b^2\right)} = \frac{\pi}{\sqrt{\lambda}} \ln\frac{r^2(a-b)^2 + m_a^2 + m_b^2 + \sqrt{\lambda}}{r^2(a-b)^2 + m_a^2 + m_b^2 - \sqrt{\lambda}}\,, \quad \text{(A.27)}$$

where we introduce the notation

$$\lambda(x, y, z) = x^2 + y^2 + z^2 - 2xy - 2xz - 2yz\,, \quad \text{(A.28)}$$

which enables us to define, for the purpose of our computation,

$$\lambda = \lambda(-r^2(a-b)^2, \alpha^2, \beta^2) = (\alpha^2 - \beta^2)^2 + 2(\alpha^2 + \beta^2)r^2(a-b)^2 + r^4(a-b)^4\,. \quad \text{(A.29)}$$

For $J^c_{m_a m_b}$ we get

$$J^c_{m_a m_b} = \frac{2\pi r^2(a-b)}{\sqrt{\lambda}}\left[\frac{1}{\sqrt{\lambda} + m_a^2 - m_b^2 + r^2(a^2 - b^2)} \times \ln\frac{a\left(\sqrt{\lambda} + r^2(a-b)^2 + m_a^2 - m_b^2\right)}{b\left(\sqrt{\lambda} - r^2(a-b)^2 + m_a^2 - m_b^2\right)} + \frac{1}{\sqrt{\lambda} + m_b^2 - m_a^2 + r^2(b^2 - a^2)} \times \ln\frac{a\left(\sqrt{\lambda} - r^2(a-b)^2 - m_a^2 + m_b^2\right)}{b\left(\sqrt{\lambda} + r^2(a-b)^2 - m_a^2 + m_b^2\right)}\right] - \frac{\pi}{a\left(b^2r^2 + m_b^2\right) - b\left(a^2r^2 + m_a^2\right)} \times \ln\frac{a\left(b^2r^2 + m_b^2\right)}{b\left(a^2r^2 + m_a^2\right)}\,. \quad \text{(A.30)}$$

The $\ln\frac{a}{b}$ terms, which apparently give divergencies when a or b goes to zero, are spurious: indeed they cancel because of the symmetrical way the function $J^c_{m_a m_b}$ appears in $a(\underline{r}; Q_1, Q_2; z_1, z_2)$, $b(\underline{r}; Q_1, Q_2; z_1, z_2)$ or $f(\underline{r}; Q_1, Q_2; z_1, z_2)$.

Let us now consider the J_{3m} integral. After performing a special conformal transformation, namely an inversion on the momentum integration variables and the other dimensional vectors and parameters, a translation and again an inversion, we arrive at integrals with a smaller number of propagators, which are calculated in the standard way. The final result reads

$$J_{3m} = \frac{2\pi}{r^2}\left\{\left(\frac{1}{r^2a^2 + m^2} - \frac{1}{r^2\bar{a}^2 + m^2}\right)\ln\frac{r^2a^2 + m^2}{r^2\bar{a}^2 + m^2} + \left(\frac{1}{r^2a^2 + m^2} + \frac{1}{r^2\bar{a}^2 + m^2} + \frac{2}{r^2a\bar{a} - m^2}\right) \times \ln\frac{(r^2a^2 + m^2)(r^2\bar{a}^2 + m^2)}{m^2r^2}\right\}. \quad \text{(A.31)}$$

With the same but a more tricky approach we can compute the J_{4mm} integral after performing a special conformal transformation; we refer to [22] for the complete calculation and final expression of this integral (see (A.66) and (A.67) of [22]). Starting from this result, we now derive another expression in such way that some spurious divergent terms (appearing when $r^2 = Q_i^2$, which corresponds to $a = 0$ or $b = 0$) explicitly cancel. Thus it allows us to use it in our numerical integration code (cf. Sects. 4 and 5). This makes the explicit expression (A.33) different from the one given in (A.67) of [22]. The resulting expression for $J_{4\mu_1\mu_2}$ is

$$J_{4\mu_1\mu_2} = \frac{1}{r^2\left(r^2\bar{z}_1^2 + \mu_1^2\right)\left(r^2\bar{z}_2^2 + \mu_2^2\right)} \times J^{\text{finite}}_{3\alpha\beta}\left(\frac{-z_1\bar{z}_1r^2 + \mu_1^2}{\bar{z}_1^2r^2 + \mu_1^2}, \frac{-z_2\bar{z}_2r^2 + \mu_2^2}{\bar{z}_2^2r^2 + \mu_2^2}, \frac{r^2\mu_1}{r^2\bar{z}_1^2 + \mu_1^2}, \frac{r^2\mu_2}{r^2\bar{z}_2^2 + \mu_2^2}, r\right) + \frac{1}{r^2\left(r^2z_1^2 + \mu_1^2\right)\left(r^2z_2^2 + \mu_2^2\right)} \times J^{\text{finite}}_{3\alpha\beta}\left(\frac{-z_1\bar{z}_1r^2 + \mu_1^2}{z_1^2r^2 + \mu_1^2}, \frac{-z_2\bar{z}_2r^2 + \mu_2^2}{z_2^2r^2 + \mu_2^2}, \frac{r^2\mu_1}{r^2z_1^2 + \mu_1^2}, \frac{r^2\mu_2}{r^2z_2^2 + \mu_2^2}, r\right), \quad \text{(A.32)}$$

with

$$J^{\text{finite}}_{3\alpha\beta}(a, b, \alpha, \beta, r) = \frac{\pi}{4}\left\{\left(\frac{8}{a-b} + \frac{2(\alpha^2 - \beta^2)}{(a-b)^2r^2}\right)\ln\frac{\alpha^2}{\beta^2}\right.$$

$$
\begin{aligned}
&+\frac{4r^2\big(-4+r^2\big(\frac{a}{a^2r^2+\alpha^2}+\frac{b}{b^2r^2+\beta^2}\big)\big)\ln\frac{b^2r^2+\beta^2}{a^2r^2+\alpha^2}}{a(a-b)br^2+b\alpha^2-a\beta^2}\\
&-2\ln\frac{\alpha^2\beta^2}{r^4}+\frac{2r^4}{(a^2r^2+\alpha^2)(b^2r^2+\beta^2)}\\
&\times\left(\ln\frac{\alpha^2\beta^2}{r^4}-2\ln\frac{\alpha^2\beta^2}{(a^2r^2+\alpha^2)(b^2r^2+\beta^2)}\right)\\
&-\Bigg(\frac{8}{(a-b)(a(a-b)br^2+b\alpha^2-a\beta^2)}\\
&\qquad\times\frac{1}{\big(-a^2r^2+b^2r^2-\alpha^2+\beta^2+\sqrt{\lambda}\big)}\Bigg)\\
&\times\Bigg[\big(-(a-b)^2r^2-\alpha^2+\beta^2+\sqrt{\lambda}\big)\\
&\times\Bigg(\frac{-a(b^2r^2+\beta^2)}{b}\ln\left(1+\frac{b^2r^2}{\beta^2}\right)\\
&+(a^2r^2+\alpha^2)\ln\frac{a^2r^2+\alpha^2}{\beta^2}\Bigg)\\
&+\big((a-b)^2r^2-\alpha^2+\beta^2+\sqrt{\lambda}\big)\\
&\times\Bigg(\frac{-b(a^2r^2+\alpha^2)}{a}\ln\left(1+\frac{a^2r^2}{\alpha^2}\right)\\
&+(b^2r^2+\beta^2)\ln\frac{b^2r^2+\beta^2}{\alpha^2}\Bigg)\Bigg]\\
&+\Bigg(\frac{\big(a^2r^2-b^2r^2+\alpha^2-\beta^2+\sqrt{\lambda}\big)^2}{(a-b)^2r^2\sqrt{\lambda}}\\
&+\frac{8(a-b)r^4\big(-4+r^2\big(\frac{a}{a^2r^2+\alpha^2}+\frac{b}{b^2r^2+\beta^2}\big)\big)}{\big((a^2-b^2)r^2+\alpha^2-\beta^2+\sqrt{\lambda}\big)\sqrt{\lambda}}\\
&+\frac{8\sqrt{\lambda}}{(a-b)(a(a-b)br^2+b\alpha^2-a\beta^2)}\Bigg)\\
&\times\ln\frac{(a-b)^2r^2+\alpha^2-\beta^2+\sqrt{\lambda}}{-(a-b)^2r^2+\alpha^2-\beta^2+\sqrt{\lambda}}\\
&+\Bigg(\frac{-\big(-a^2r^2+b^2r^2-\alpha^2+\beta^2+\sqrt{\lambda}\big)^2}{(a-b)^2r^2\sqrt{\lambda}}\\
&+\frac{8(a-b)r^4\big(-4+r^2\big(\frac{a}{a^2r^2+\alpha^2}+\frac{b}{b^2r^2+\beta^2}\big)\big)}{\big((-a^2+b^2)r^2-\alpha^2+\beta^2+\sqrt{\lambda}\big)\sqrt{\lambda}}\Bigg)\\
&\times\ln\frac{-(a-b)^2r^2-\alpha^2+\beta^2+\sqrt{\lambda}}{(a-b)^2r^2-\alpha^2+\beta^2+\sqrt{\lambda}}\\
&+\Bigg[\frac{16r^2}{\sqrt{\lambda}}+\frac{2r^2\big(4+r^2\big(-\big(\frac{1}{a^2r^2+\alpha^2}\big)-\frac{1}{b^2r^2+\beta^2}\big)\big)}{\sqrt{\lambda}}\\
&-8\frac{(a^2-b^2)r^2+\alpha^2-\beta^2}{(a-b)\sqrt{\lambda}}-\frac{2\sqrt{\lambda}}{(a-b)^2r^2}\Bigg]\\
&\times\ln\frac{(a-b)^2r^2+\alpha^2+\beta^2+\sqrt{\lambda}}{(a-b)^2r^2+\alpha^2+\beta^2-\sqrt{\lambda}}\Bigg\}\,,
\end{aligned}
\tag{A.33}
$$

where appropriate additional $\ln r^2$ terms have been introduced in order to write the final result as made of logarithms of dimensionless quantities. The difference between these two expressions only involves terms proportional to $\ln r^2$, in accordance with the dimensional regularization, since $J_{3\alpha\beta}$ is a divergent integral. However, at the level of the final result for $J_{4\mu_1\mu_2}$, which is both UV and IR finite, these additional terms of course cancel each other.

References

1. E.A. Kuraev, L.N. Lipatov, V.S. Fadin, Phys. Lett. B **60**, 50 (1975)
2. E.A. Kuraev, L.N. Lipatov, V.S. Fadin, Sov. Phys. JETP **44**, 443 (1976)
3. E.A. Kuraev, L.N. Lipatov, V.S. Fadin, Sov. Phys. JETP **45**, 199 (1977)
4. Y.Y. Balitskii, L.N. Lipatov, Sov. J. Nucl. Phys. **28**, 822 (1978)
5. V.N. Gribov, L.N. Lipatov, Yad. Fiz. **15**, 781 (1972)
6. V.N. Gribov, L.N. Lipatov, Sov. J. Nucl. Phys. **15**, 438 (1972)
7. G. Altarelli, G. Parisi, Nucl. Phys. B **126**, 298 (1977)
8. Y.L. Dokshitzer, Sov. Phys. JETP **46**, 641 (1977)
9. Y.L. Dokshitzer, Zh. Eksp. Teor. Fiz. **73**, 1216 (1977)
10. J. Bartels, A. De Roeck, H. Lotter, Phys. Lett. B **389**, 742 (1996)
11. S.J. Brodsky, F. Hautmann, D.E. Soper, Phys. Rev. Lett. **78**, 803 (1997)
12. S.J. Brodsky, F. Hautmann, D.E. Soper, Phys. Rev. Lett. **79**, 3544 (1997) [Erratum]
13. J. Kwiecinski, L. Motyka, Phys. Lett. B **462**, 203 (1999)
14. J. Bartels, C. Ewerz, R. Staritzbichler, Phys. Lett. B **492**, 56 (2000)
15. J. Kwiecinski, L. Motyka, Eur. Phys. J. C **18**, 343 (2000)
16. V.P. Goncalves, M.V.T. Machado, W.K. Sauter, hep-ph/0611171
17. M. Boonekamp, A. De Roeck, C. Royon, S. Wallon, Nucl. Phys. B **555**, 540 (1999)
18. J. Kwiecinski, L. Motyka, Phys. Lett. B **438**, 203 (1998)
19. B. Pire, L. Szymanowski, S. Wallon, International Conference on Linear Colliders (LCWS 04), Paris, France, 19–24 April 2004, in: Paris 2004, Linear Colliders, vol. 1, pp. 335–340
20. B. Pire, L. Szymanowski, S. Wallon, 10th International Conference on Structure of Baryons (Baryons 2004), Palaiseau, France, 25–29 October 2004, Nucl. Phys. A **755**, 626 (2005)
21. B. Pire, L. Szymanowski, S. Wallon, 11th International Conference on Elastic and Diffractive Scattering, Blois, France, 15–20 May 2005, in: Towards High Energy Frontiers, ed. by M. Haguenauer et al., pp. 373–376
22. B. Pire, L. Szymanowski, S. Wallon, Eur. Phys. J. C **44**, 545 (2005)
23. R. Enberg, B. Pire, L. Szymanowski, S. Wallon, Eur. Phys. J. C **45**, 759 (2006)
24. R. Enberg, B. Pire, L. Szymanowski, S. Wallon, PHOTON 2005, Warsaw, 30 August–8 September 2005, Acta Phys. Polon. B **37**, 847 (2006)
25. B. Pire, M. Segond, L. Szymanowski, S. Wallon, Phys. Lett. B **639**, 642 (2006)
26. L. Mankiewicz, G. Piller, Phys. Rev. D **61**, 074013 (2000)
27. D.Y. Ivanov, R. Kirschner, Phys. Rev. D **58**, 114026 (1998)
28. D.Y. Ivanov, R. Kirschner, A. Schafer, L. Szymanowski, Phys. Lett. B **478**, 101 (2000)

29. D.Y. Ivanov, R. Kirschner, A. Schafer, L. Szymanowski, Phys. Lett. B **498**, 295 (2001) [Erratum]
30. A. Ivanov, R. Kirschner, Eur. Phys. J. C **29**, 353 (2003)
31. A.D. Martin, M.G. Ryskin, T. Teubner, Phys. Rev. D **55**, 4329 (1997)
32. A.D. Martin, M.G. Ryskin, T. Teubner, Phys. Rev. D **56**, 3007 (1997)
33. A.D. Martin, M.G. Ryskin, T. Teubner, Phys. Rev. D **62**, 014 022 (2000)
34. D.Y. Ivanov, A. Papa, Nucl. Phys. B **732**, 183 (2006)
35. D.Y. Ivanov, A. Papa, hep-ph/0610042.
36. V.M. Budnev, I.F. Ginzburg, G.V. Meledin, V.G. Serbo, Phys. Rep. **15**, 181 (1974)
37. I.F. Ginzburg, S.L. Panfil, V.G. Serbo, Nucl. Phys. B **284**, 685 (1987)
38. D.Y. Ivanov, M.I. Kotsky, A. Papa, Eur. Phys. J. C **38**, 195 (2004)
39. P. Ball, V.M. Braun, Y. Koike, K. Tanaka, Nucl. Phys. B **529**, 323 (1998)
40. M. Vanderhaeghen, P.A.M. Guichon, M. Guidal, Phys. Rev. D **60**, 094 017 (1999)
41. S.V. Goloskokov, P. Kroll, Eur. Phys. J. C **42**, 281 (2005)
42. V.M. Braun, G.P. Korchemsky, D. Mueller, Prog. Part. Nucl. Phys. **51**, 311 (2003)
43. S. Bethke, J. Phys. G **26**, R27 (2000)
44. ILC, Basic Conceptual Design Report, http://www.linearcollider.org
45. LDC outline document, http://www.ilcldc.org
46. M. Davier, M.E. Peskin, A. Snyder, hep-ph/0606155
47. G.T. Bodwin, E. Braaten, J. Lee, C. Yu, Phys. Rev. D **74**, 074 014 (2006)
48. L. Lewin, Polylogarithms and Associated Functions (North-Holland, New York, 1981)
49. B. Clerbaux, M.V. Polyakov, Nucl. Phys. A **679**, 185 (2000)
50. A.P. Bakulev, S.V. Mikhailov, Phys. Lett. B **436**, 351 (1998)
51. V.P. Goncalves, W.K. Sauter, Eur. Phys. J. C **44**, 515 (2005)
52. V.P. Goncalves, W.K. Sauter, Phys. Rev. D **73**, 077 502 (2006)
53. S. Braunewell, C. Ewerz, Phys. Rev. D **70**, 014 021 (2004)
54. A.N. Vasil'ev, The Field Theoretic Renormalization Group in Critical Behavior theory and Stochastic Dynamics (Chapman and Hall/CRC, 2004)